大麻素受體對於齒狀迴顆粒細胞抑制性調控之影響

Cannabinoid receptor-mediated inhibitory control of dentate granule cells

研究生：高敏華 (Min-Hua Kao)

指導教授：連正章 博士 (Cheng-Chang Lien, M.D., Ph.D.)

國立陽明大學

神經科學研究所

碩 士 論 文

Institute of Neuroscience

National Yang-Ming University

Master Thesis

中華民國一〇五年五月

May, 2016

誌謝

快三年的研究成果獻給在此期間為實驗犧牲的所有生命，謝謝。

首先，非常感謝指導教授連老師的指導，並謝謝老師提供優渥的研究環境，充足的資源，最後謝謝老師花了很多時間幫我修改論文。謝謝大鈞與阿詹充滿耐心的教導我學會電生理，謝謝政達在實驗及技術部分的指導與幫忙，謝謝蝦哥在論文方面幫了我很大的忙，也謝謝小捲在口試期間幫忙我許多，謝謝 Simon 在實驗上的幫忙，謝謝 CJ、TYY、陳勤霖、林昱伶、Simon、Davis 為實驗室生活帶來許多樂趣，也謝謝實驗室的大家的幫忙。謝謝張穎柔和魏敬容在我實驗不順遂時聽我吐口水，謝謝莊凱彬不辭辛勞的陪伴，最後，謝謝爸爸、媽媽與家人的支持，讓我能夠完成學業。

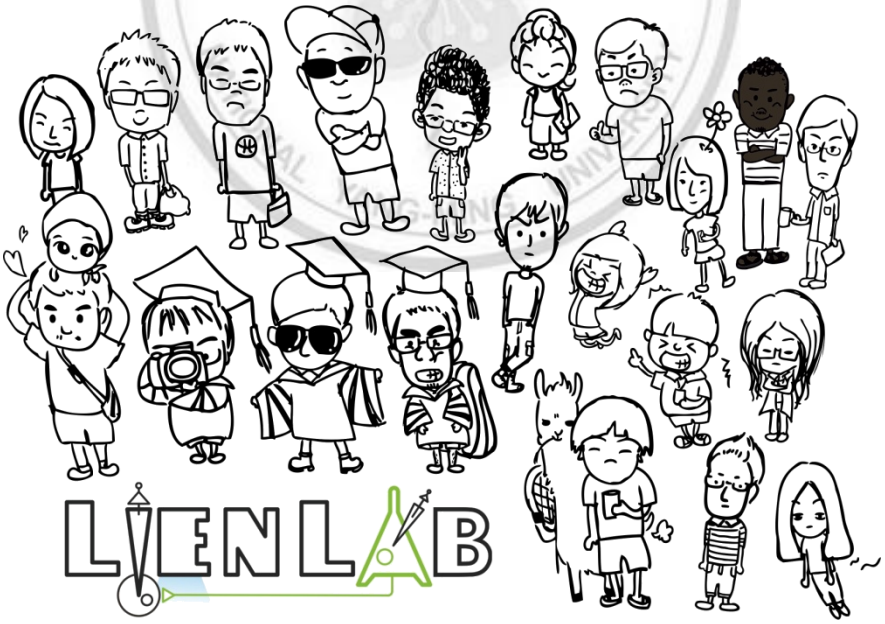

高敏華　謹致於

國立陽明大學神經科學研究所

中華民國一百零五年五月

中文摘要

海馬迴為學習與記憶功能重要的核區。在海馬迴中的齒狀迴結構是負責處理訊息由大腦皮質區傳遞至海馬迴的第一站。在齒狀迴中主要細胞群「顆粒細胞」受到來自不同種類的 γ-胺基丁酸抑制性神經細胞嚴密地調控，而此抑制性調控對於大腦辨識相似的事件、物品之功能扮演非常重要的角色。然而，這些不同種類的 γ-胺基丁酸抑制性神經細胞在被內嗅皮質層傳遞至齒狀迴之穿緣通路活化時，如何調控顆粒細胞仍不清楚。我們發現當刺激穿緣通路時顆粒細胞的活性受到極為強烈的抑制，當阻斷 γ-胺基丁酸抑制性神經傳導物質後，顆粒細胞的活化閾值降低，相較於阻斷 γ-胺基丁酸抑制性神經傳導物質前，可增加將近三倍大的顆粒細胞群尖峰電位。在齒狀迴中，其中一種 γ-胺基丁酸抑制性神經細胞會表現大麻素受體，藉由大麻素受體之促效劑活化大麻素受體會減少此類 γ-胺基丁酸抑制性神經細胞的抑制性神經傳導。相反地，我們發現給予大麻素受體之促效劑會增加顆粒細胞所接受到之抑制性神經傳導及減少顆粒細胞之群尖峰電位，並進一步證明此現象是透過 γ-胺基丁酸抑制性神經傳導物質所導致。因此，我們推論大麻素受體之促效劑可能是透過降低對於抑制性神經細胞的抑制，促使抑制性神經細胞解除抑制進而增加對於顆粒狀細胞之抑制性神經傳導。除此之外，我們也發現大麻素受體之促效劑會增強籃狀細胞之活性，但籃狀細胞之活性增加並不是造成顆粒細胞群尖峰電位降低的主要原因。

Abstract

The hippocampus plays an important role in learning and memory. The dentate gyrus (DG) serves as a primary gateway to the hippocampus, filtering information from the cortex and sending output to other hippocampal areas. The largest neural population in the DG, granule cells (GCs), are under tight control by various types of GABAergic interneurons (INs) and the inhibitory control is crucial for sparse coding and pattern separation. However, how these different types of INs regulate the activity of GCs in response to cortical inputs remains unclear. We found that GCs receive remarkably strong inhibition. The threshold of GCs for spiking decreases and the GC population spikes (pSpikes) increase almost three-fold after blocking $GABA_A$ receptors. In the DG, cannabinoid type 1 receptors (CB_1Rs) are expressed on some of the GABAergic INs. The CB_1R activation by CB_1R agonist WIN 55,212-2 reduces GABAergic transmission of the CB_1R-expressing INs. In contrast, we found that WIN 55,212-2 enhances the inhibitory currents GC received and decreases the GC pSpikes through GABAergic transmission. These results suggest a CB_1R-mediated disinhibitory microcircuits in the DG. Furthermore, we also observed that WIN 55,212-2 increases the activity of basket cells (BCs). However, the enhancement of BC activity does not contribute to the WIN 55,212-2-mediated suppression of GC pSpikes.

Contents

Abbreviations

AAV: adeno-associated virus
AP: action potential
BC: basket cell
CB_1R: cannabinoid type 1 receptor
CB_1R-KO: cannabinoid type 1 receptor knock-out
CCK: cholecystokinin
DG: dentate gyrus
DIO: double-floxed inverted open reading frame
eNpHR: enhanced Natronomonas halorhodopsin
EPSC: excitatory postsynaptic current
eYFP: enhanced yellow fluorescent protein
FS: fast-spiking
fEPSP: field excitatory postsynaptic potential
GC: granule cell
GCL: granule cell layer
HICAP: hilar commissural associational pathway-associated
HIPP: hilar perforant pathway-associated
I/E ratio: the ratio of inhibitory-excitatory conductance
IML: inner molecular layer
IN: interneuron
LPP: lateral perforant pathway
ML: molecular layer
MML: medial molecular layer
MPP: medial perforant pathway
OML: outer molecular layer
PP: perforant pathway
PPR: paired-pulse ratio
pSpike: population spike
PV: parvalbumin
R_{in}: input resistance
SST: somatostatin
Sub: subiculum
TML: total molecular layer
VIP: vasoactive intestinal polypeptide
WT: wild-type

Introduction

The hippocampus

In human, the hippocampus, named after its seahorse-like structure in Greek, is located in the medial temporal lobe and this structure is well preserved between mammalian brains (Colombo and Broadbent, 2000). In rodent brains, it is larger and just under the neocortex (Knierim, 2015). The hippocampus is a complex and highly specialized structure. It receives various inputs including the major inputs from entorhinal cortex and others from the medial septum, locus coeruleus, raphe nucleus, nucleus reuniens, and amygdala (Amaral et al., 2007; Andersen et al., 2007; Knierim, 2015). The output projections of the hippocampus will be back to the entorhinal cortex and to other brain regions, such as nucleus accumbens, amygdala, and prefrontal cortex (Knierim, 2015). The hippocampus can be subdivided into two parts, the dentate gyrus (DG) and Cornu Ammonis (CA). The major input from the entorhinal cortex first projects to the DG through the perforant pathway (PP). The principal cells in the DG, granule cells, project to the CA3 region. Then, the principal cells, pyramidal cells, in the CA3 area project to the CA1 region. Finally, the pyramidal cells in the CA1 area project back to the entorhinal cortex. It's thus so-called "trisynaptic loop" (Amaral et al., 2007). Besides the principal cells in the hippocampus, there are various GABAergic INs providing local inhibition for

regulating those principal cells or sending long-range projections to other brain regions (Caputi et al., 2013). These delicate and complicated structures build up the hippocampus and play an important role in memory formation, spatial learning, emotion and cognitive function (Scoville and Milner, 1957; O'Keefe and Nadel, 1978; Moser et al., 2008; Chersi and Burgess, 2015; Strange et al., 2014; Malykhin and Coupland, 2015).

The dentate gyrus

As the first gate of the hippocampus, the DG is an extremely laminated structure, which can be divided into three layers (Amaral et al., 2007). The somata of the GCs densely compact together to form the granule cell layer (GCL). The molecular layer (ML) is mostly composed of the dendrites of the GCs and input fibers from various brain regions. There is relatively less density of the cell bodies in this layer. The ML can be further classified into three parts, the inner ML (IML), medial ML (MML) and outer ML (OML) (Cajal, 1893). Roughly speaking, the first one-third of the area from the GCL is the IML occupied by the axonal projections of the hilar mossy cells (Scharfman and Myers, 2012; Hsu et al, 2015). The middle one-third of the area is the MML occupied by the projections from the medial PP (MPP) while the outer one-third of the area is the OML occupied by the projections from the lateral PP (LPP). On the other side of the GCL is the hilus and there are not only the axons of

the GCs projecting to the CA3 area but also the somata of the mossy cells and hilar interneurons (Amaral et al., 2007).

The DG is the first relay link of the trisynaptic loop and acts as the gatekeeper of the hippocampus to control information transfer from the cortex to the hippocampus (Amaral et al., 2007; Treves et al., 2008). Only a small portion of GC populations can elite action currents while receiving strong and massive inputs from the cortex, called sparse coding (Chawla et al., 2005; Pernía-Andrade and Jonas, 2014). It prevents the overwhelm excitation and seizures in the hippocampus (Behr et al., 1998; Coulter and Carlson, 2007). The feature of the sparse coding is important for spatial learning and pattern separation (Leutgeb et al., 2007; Moser et al., 2008; Aimone et al., 2011).

Interneurons in the DG

The mechanisms of sparse coding may result from the intrinsic properties of the GCs and the regulation of inhibitory circuits. The membrane properties of the GCs are remarkably passive. Synaptic inputs strongly attenuate along the dendrites of the GCs since there are no active conductances in the GCs dendrites (Schmidt-Hieber et al., 2007; Krueppel et al., 2011). Furthermore, the resting membrane potentials of the GCs are relatively negative compared with pyramidal cells. On the other hand, the GCs receive powerful feedforward and feedback inhibition from local interneurons (Cobb et al., 1995; Pouille and Scanziani, 2001; Nitz and McNaughton, 2004; Ewell

and Jones, 2010; Dieni et al., 2013), as well as the tonic inhibition from the high extracellular GABA concentration (Nusser and Mody, 2002; Stell and Mody, 2002). Interneurons in the brains exhibit high diversity in terms of their morphologies, electrical properties and neurochemical markers. In the DG, there are five major types of INs classified by their axonal arborizations. First of all, the axons of parvalbumin (PV)-expressing fast-spiking (FS) BCs target the somata of the GCs in the GCL and BCs provide strong inhibition and efficiently control the action potential generation of the GCs. The others target the dendrites of the GCs, such as somatostatin (SST)-expressing hilar perforant pathway-associated (HIPP)-like cells projecting to the distal dendritic region of GCs (OML) and cholecystokinin (CCK)-expressing hilar commissural associational pathway-associated (HICAP)-like cells projecting to the GCs proximal dendrites (IML). In addition, the axons of total molecular layer (TML)-like cells are over the entire ML. Finally, the somata and their neurites all located in the ML are classified into the molecular layer (ML)-like cells (Halasy and Somogyi, 1993; Hosp et al., 2014; Hsu et al., 2015).

Endocannabinoid receptor-expressing INs in the DG

Endocannabinoids are one of the key synaptic modulators in the brain. Endocannabinoids synthesized from postsynaptic neurons target presynaptic CB_1R to suppress the neurotransmitter release. CB_1Rs are G protein-coupled receptors and

through two main molecular mechanisms to regulate the neurotransmitter release. For the mechanism underlying the short-term plasticity, CB_1R activation inhibits the presynaptic Ca^{2+} influx through voltage-gated Ca^{2+} channels via the βγ subunits of G proteins (Brown et al., 2003; Wilson et al., 2001). For mechanism underlying the long-term plasticity, CB_1R activation involves inhibition of adenylyl cyclase, downregulation of the cyclic adenosine monophosphate and protein kinase A pathway through the α subunits of G proteins (Heifets and Castillo, 2009; Castillo et al., 2012). In the DG, the highest density of CB_1R immunoreactivity is in the IML (Tsou et al., 1998; Egertová and Elphick, 2000; Monory et al., 2006). For the glutamatergic inputs to the DG, CB_1Rs are exclusively expressed in mossy cell terminals but not from the PP (Monory et al., 2006, Chiu and Castillo, 2008; Chancey et al., 2014). As GABAergic inputs, CB_1Rs are known to be expressed in CCK^+ INs and the axons are located in the IML, which also called HICAP cells (Somogyi et al., 1984; Nunzi et al., 1985; Katona et al., 1999; Tsou et al., 1999). Aside from the IML, CB_1R-expressing axons exhibit across the entire ML while deleted CB_1Rs in glutamatergic terminals (Monory et al., 2006). TML cells that do not express CCK are another type of CB_1R-expressing INs (Yu et al., 2015).

Inhibitory circuits for the signal processing in the DG

In the brain, neurons cluster together and respond to the same cognitive function (Shatz, 1990). They might receive the similar inputs and process the information from upstream brain regions, and then send outputs to downstream regions. The information is also regulated by local GABAergic INs. From the tiny tips of dendritic process to soma, the axon initial segments and extensive axonal projections, the excitatory principal neurons are innervated by GABAergic synapses from various types of INs. These INs target different parts of principal cells to specifically regulate their activities and plasticity (Miles et al., 1996; Royer et al., 2012). The threshold and timing of spikes in principal cells are fine-tuned by GABAergic INs through the feedforward and feedback inhibition (Pouille et al., 2001; Pouille and Scanziani, 2004; Jang et al., 2015). INs also contribute to neuronal synchronization and generate oscillations (Buzsa´ki and Draguhn, 2004; Klausberger and Somogyi, 2008; Allen and Monyer, 2015). Similarly, inhibition from multiple types of INs controls the GC activities and involves in the sparse coding of GCs (Acsády and Káli, 2007; Coulter and Carlson, 2007; Dieni et al., 2013; Yu et al., 2013). However, the role of specific types of GABAergic INs in the DG signal processing remains unclear.

The aims

Understanding the neural circuits helps figure out how the brain process the information and it's essential to understanding its function. The INs are a small portion of neurons in the brain but tightly control the activity of principal cells. INs display high diversity in the morphology and the electrical properties (McBain and Fisahn, 2001). In the present study, we aimed to explore how different types of INs regulate the GC input-output transformation in the DG. Moreover, we investigated the regulatory role of endocannabinoid signaling in the modulation of INs onto the GC in the DG.

國立陽明大學 NATIONAL YANG-MING UNIVERSITY

Materials and Methods

Animals

Wild-type (WT) C57BL/6 mice were provided by the Animal Center of National Yang-Ming University. The CB_1R-knock-out (KO) mice were derived from a stock of genotyped animals that were provided by Dr. Zimmer (Zimmer et al., 1999). For optogenetic experiments, transgenic hemizygote mice were used. The *Pvalb-cre* mice were purchased from the Jackson Laboratory (stock no. 008069; The Jackson Laboratory, Bar Harbor, ME, USA). All mice were bred onto the C57BL/6J genetic background. Mice of both sexes of the above strains (2-4 months) were used for all the experiments. Animal procedures were performed in accordance with the National Institutes of Health's *Guide for the Care and Use of Laboratory Animals*. The experimental protocol was reviewed and approved by the Institutional Animal Care and Use Committee of National Yang-Ming University.

Virus and stereotaxic injection

To selectively silence PV^+ INs in the DG, we used an adeno-associated virus-5 (AAV5) carrying a Cre-inducible enhanced Natronomonas halorhodopsin 3.0 (eNpHR3.0)-enhanced yellow fluorescent protein (eYFP) transgene AAV5-EF1α-DIO-eNpHR3.0-eYFP produced by the University of North Carolina

Vector Core Facilities (Chapel Hill, NC, USA).

Mice (at postnatal days >30) were anesthetized with 4% isoflurane (vol/vol; Halocarbon Laboratories, North Augusta, SC, USA) in 100% oxygen in an induction chamber (air flow rate: 4 mL/min), and their heads were shaved for further operation. Mice were placed onto the stereotaxic frame (David Kopf Instruments, Tujunga, CA). The mouths and noses of the mice were covered by an anesthetizing mask, supplied with approximately 1.5% isoflurane air flow (4 mL/min). A heating pad (EG-220B, E-GMED Health Co., Ltd.) was placed below the mice to keep the body temperature constant (34℃). After securing the head with two ear bars, 75% ethanol was used to sterilize the surgical area and the eyes were protected by ophthalmic gel. A midline scalp incision (~1 cm) was made with scissors and the skin pulled aside to expose the skull. A small craniotomy (coordinates from Bregma: anteroposterior (AP): -3.4 mm; mediolateral (ML): ±2.8 mm) was made directly over the ventral hippocampus. The viral vector was delivered through the craniotomy to the 2 locations within the ventral hippocampus (dorsoventral (DV): -4.4 and -4.2 mm), using a 10-μL NanoFil syringe (World Precision Instruments, Sarasota, FL, USA) and a 35-gauge beveled metal needle. Injection volume (0.5 μL at each location) and flow rate (0.1 μL/min) were controlled with a nanopump Controller (KD Scientific, Holliston, MA, USA). After viral injection, the needle was left in place 0.2 mm above the injection sites for 10 min

before it was withdrawn slowly. The incision was closed by suturing and mice were placed back to the home cage for recovery. All animals were allowed at least 6 weeks of rest before the next experimental stage was commenced, ensuring complete recovery and sufficient gene expression.

Electrophysiology

Animals were killed by rapid decapitation by appropriately trained researchers. In brief, their brains were rapidly removed and 400 μm-thick horizontal sections were prepared with a vibratome (DTK-1000; Dosaka) using ice-cold sucrose based solution containing the following (in mM): 87 NaCl, 25 $NaHCO_3$, 1.25 NaH_2PO_4, 2.5 KCl, 10 glucose, 75 sucrose, 0.5 $CaCl_2$, and 7 $MgCl_2$, bubbled with 95%O_2/5%CO_2, pH7.4. Slices were incubated in the same solution at 34℃ for at least 30 min and then transferred to oxygenated ACSF containing the following (in mM): 125 NaCl, 25 $NaHCO_3$, 1.25 NaH_2PO_4, 2.5 KCl, 25 glucose, 2 $CaCl_2$, and 1 $MgCl_2$. During experiments, slices were placed in a recording chamber and continuously superfused (~3.5 ml/min) with oxygenated ACSF.

GCs and INs in the DG were visually identified using infrared differential interference contrast microscope (IR-DIC) (Olympus BX51WI) coupled with an infrared-sensitive CCD camera (Hamamatsu, C7500-50). The PP fibers were stimulated for 0.1 ms with constant current (range of 0.01-1 mA) using a monopolar

electrode placed in the subiculum to avoid the direct activation of DG IN axons. Most experiments were performed at the nearly maximal stimulus intensity. Field recordings were performed with ACSF-filled patch pipettes (with a resistance of <1 MΩ). Cell-attached recordings (pipette resistance 8-10 MΩ) were made to detect spike responses. Whole-cell patch-clamp recordings were made with an Axopatch 200B amplifier or Multiclamp 700B amplifier (Molecular Devices). Recording electrodes (3-6 MΩ) were pulled from borosilicate glass capillaries (outer diameter, 1.5 mm; 0.32 mm wall thickness; Harvard Apparatus). Pipette capacitances and series resistance were compensated (100% in current clamp and 70% in voltage clamp). Signals were filtered at 4 or 5 kHz using the 4-pole low-pass Bessel filter sampled at 10 kHz using a digitizer (Digidata 1440A; Molecular Devices). Pulse sequences were generated by pCLAMP version 10.2 or 10.3 (Molecular Devices). The recording temperature was 34 ± 2℃ using a single channel heater controller (TC-324B equipped with a SH-27B solution on-line heater, Warner Instrument Corp.). The eNpHR-eYFP expression pattern was confirmed by epifluorescence. Axonal fibers expressing eNpHR3.0-eYFP were stimulated with amber light (590 nm; LED4D162, controlled by DC4104 driver, Thorlabs), which was delivered through the objective.

Calibration of input strength for GC activation

The input strength was calibrated in all experiments as described previously (Pouille

et al., 2009). Briefly, the input strength is a value that represents the number of active presynaptic neurons and is normalized from 0 to 1, permitting the comparison of stimulus intensities across slices. We used two parameters to calculate the input strength: the initial slope (20-50%) of field excitatory postsynaptic potential (fEPSP), which is proportional to the number of activated PP fibers, and the area under the pSpike, which is proportional to the number of active GCs around the DG recording sites (Fig. 1). Therefore, all the input strengths shown in this study were performed in the presence of two field recording electrodes: one placed in the ML for fEPSPs, and the other in the GCL for pSpikes. The fEPSP slope evoked at any given stimulus intensity was normalized to the fEPSP slope elicited by a stimulus intensity that resulted in a pSpike at 95% of its maximum (which means 95% of local spiking GCs are recruited). The value of such normalized fEPSP is the input strength. Thus, an input strength of 1.0 means that the number of stimulated PP fibers can recruit 95% of local spiking GCs and an input strength of 0.1 means that the number of stimulated PP is one-tenth of the number at input strength 1.0. For each slice, the input strength was determined under control conditions. The amplitude of the pSpike had to remain stable for at least 10 min before the input strength was calibrated.

Threshold and activation curves

Neurons were recorded in the cell-attached configuration, and the PP was stimulated

at different intensities to determine the threshold input strength, which evoked a 50% of maximum spike in the recorded cells. Five to ten stimuli were tested at each intensity to calculate spiking probability. The 50% spiking probability of individual neurons was determined by fitting their spiking probability plotted against input strength with a sigmoid function $Y = 100/[1+10\text{^}p(x_0\text{-}x)]$, where x_0 is the input strength at 50% spiking probability, and p is the slope at x_0 (Pouille et al., 2001).

Chemicals and drugs

The majority of whole-cell patch-clamp recordings were made with the intracellular solution containing the following (in mM): 136.8 K-gluconate, 7.2 KCl, 0.2 EGTA, 4 MgATP, 10 HEPES, 7 Na_2-phosphocreatine, 0.5 Na_3GTP (pH 7.3 with KOH), and 0.4% biocytin (wt/vol). To measure the inhibitory (I)-excitatory (E) conductance ratio, Cs-based intracellular solution was used, containing the following (in mM): 121.5 $CsMeSO_3$, 0.1 EGTA, 4 $MgCl_2$, 13.5 $CsCl_2$, 10 HEPES, 5 QX-314 bromide, 2 Na_2ATP, 10 Na_2-phosphoreatine, 0.3 Na_3GTP. All experiments were performed in the presence of the 20 μM *N*-methyl-d-aspartate (NMDA) receptors antagonist D-2-amino-5-phosphonopentanoate (D-APV, Tocris) and 1 μM $GABA_B$ receptor antagonist CGP55845 (Tocris). In a subset of experiments, one or more of the following antagonists was also added to the ACSF: 2 mM kynurenic acid (Sigma) to block AMPA and NMDA receptors; 1 μM gabazine (Tocris) to block $GABA_A$

receptors. The CB_1R agonist WIN 55,212-2 (5 μM, Tocris or Sigma) and the antagonist AM251 (5 μM, Tocris) were dissolved in DMSO. Total DMSO in the ACSF was maintained below 0.025% in all experiments.

Biocytin filling and *post-hoc* morphological reconstruction

To identify the recorded neurons (filled with 0.4% biocytin), brain slices were fixed overnight with 4% paraformaldehyde (wt/vol) in phosphate-buffered saline (PBS). After washing with PBS 3 times, slices were incubated with streptavidin-conjugated Alexa Fluor 488 (1: 400; Life Technologies) in PBS and 0.3% Triton X-100 (vol/vol; USB Co., Cleveland, OH, USA) overnight at 4℃. After washing 6 times with PBS, slices were mounted onto slides with mounting medium Vectashield (Vector Laboratories, Burlingame, CA, USA). Labeled cells were imaged by a confocal/two-photon laser excitation microscope (Leica SP5 module, Leica Microsystems). For 3D reconstruction of biocytin-labeled cells, high-resolution two-photon images of neurons were acquired. Labeled neurons were examined by a two-photon microscope using a pulsed titanium: sapphire laser (Chameleon-Ultra II tuned to 800 nm; Coherent) attached to a Leica DM6000 CFS that was equipped with a 20×/1.0 numerical aperture water-immersion objective (objective type HCX APO L). The morphology of the cells was reconstructed from a stack of 137-198 images per cell (voxel size, 0.5-0.65 μm in the x-y plane; 1.98 μm along the z-axis). Image stacks

belonging to one cell were imported into the Neuromantic 1.6.3 software (Myatt et al., 2012) for 3D reconstruction. To quantify the axonal distribution, we counted the number of intersections made by the axons with lines running parallel to the border between the GCL and the molecular layer and interspaced by 10 µm (Liu et al., 2014).

Data analysis and statistics

Data were analyzed using Clampfit version 10.2 or 10.3 (Molecular Devices) and Prism version 5.0 or 6.0 (GraphPad Software, La Jolla, CA, USA). The input resistance (R_{in}) was measured by the ratio of the steady-state (the last 100 ms) voltage response versus the injected 1 s hyperpolarizing (-50 pA) current pulse. The threshold was measured as the voltage at which the first derivative of voltage exceeded the threshold (20 V/s). Peak amplitude of action potentials (APs) was measured from threshold to the peak potential. Half-duration of action potentials was measured at the two points during the rise and decay phase halfway between threshold and peak. The paired-pulse ratio (PPR) was defined as the ratio of the amplitude of the second excitatory postsynaptic current (EPSC) to the amplitude of the first EPSC. The magnitude of pSpike was quantified by the area, which reflects the number of GCs that spike synchronously to PP stimulation (Fig. 1A). Data are presented as mean ± SEM. Error bars in the figures equal SEM and are plotted only when they exceeded the respective symbol size. Because the normality of underlying distributions of

variables in both groups is not known (Walker, 2002), we determined statistical significance by the Wilcoxon signed rank test (pairwise comparisons). Comparisons between multiple groups were tested by one-way ANOVA (with Bonferroni *post hoc* test) or two-way ANOVA test (with Bonferroni *post hoc* test).

Results

GC activity is tightly controlled by GABAergic inhibition

In order to investigate how GABAergic transmission impacts on the GC input-output transformation, we first tested the role of $GABA_A$ receptor-mediated inhibition onto the spiking probabilities that GCs generated in response to afferent stimulation. We placed a stimulation electrode on the subiculum (Sub) to stimulate the cortical input including the MPP and LPP. In order to normalize the stimulus intensity across slices, we simultaneously recorded pSpikes in the GCL and corresponding fEPSPs in the OML over a range of stimulus intensities (Fig. 1A). We plotted the pSpike areas against the fEPSP slopes and all the data points were fit with a sigmoid function to acquire the maximum pSpike (Fig. 1B). The normalized stimulus intensity, referred as input strength in this study, was obtained by normalizing the obtained fEPSP slope to the fEPSP slope, which can evoke 95% of the maximum pSpike (see equation in Fig. 1A and Fig. 1B). Next, we recorded the spikes in the cell-attached configuration from individual GCs located in the outer one-third of the GCL. Notably, the spiking probability of individual GCs was enhanced with the increase of stimulus intensity (Fig. 1C). Finally, we obtained the activation curve of single GCs (Fig. 1D, see Materials and Methods) and defined the threshold input strength (the input strength which could evoke 50% spiking probability in individual GCs, see Materials and

Methods). We found that blocking GABAergic transmission with the $GABA_A$ receptor antagonist gabazine (1 μM) increased the spiking probability of individual GCs with the same input strength (Fig. 2A). As a result, the activation curves (n = 10; Fig. 2B) were shifted to the left after gabazine application (n = 9; Fig. 2C) and the threshold input strength of GCs was significantly reduced (n = 6; 0.7 ± 0.1 in the control group and 0.4 ± 0.1 in the gabazine group; $p < 0.05$, Wilcoxon signed rank test; Fig. 2D). Furthermore, the application of gabazine also transformed a subpopulation of non-spiking (NS) GCs into spiking GCs (NS : S, n = 7: 9 in the control group and 1: 9 in the gabazine group; Fig. 2E).

To address whether GABAergic inhibition could impact on the input-output relationship of GC population, we quantified the pSpike areas at the same stimulus intensity after gabazine application. We found that the pSpike areas were enhanced among increasing stimulus intensities (Fig. 3A) and reached about 2.7-fold of the maximum pSpike areas before gabazine application (264.3%; n = 5; $p < 0.001$, two-way repeated-measures ANOVA; Fig. 3B). GCs received EPSCs with coherence in theta frequency band while received IPSCs with coherence in the gamma frequency band *in vivo* (Pernía-Andrade and Jonas, 2014). We thus stimulated PPs with 10-Hz (theta) or 30-Hz (gamma) trains to test how GABAergic inhibition regulates GCs in response to series of cortical inputs. The GC pSpike areas robustly increased at 10- or

30-Hz trains and it is frequency dependent ($n = 5$; $p < 0.001$, two-way ANOVA; Fig. 3C). At the late phase of 30-Hz trains, the pSpikes significantly enhanced rather than those at 10-Hz ($p < 0.05$, *post hoc* Bonferroni's test; Fig. 3D). In summary, the $GABA_A$ receptor-mediated transmission provided an extremely strong inhibition onto GC populations.

The CB_1R agonist WIN 55,212-2 reduces GC pSpikes by modulating GABAergic transmission

GABAergic INs in the DG can be classified into five major types according to their morphological and electrophysiological features (Hosp et al., 2014). Previous studies have shown that dendrite- and soma-targeting INs differentially control the activities of principal cells (Miles et al., 1996; Royer et al., 2012; Liu et al., 2014). Dendrite-targeting INs regulate the dendritic excitability and synaptic plasticity while soma-targeting INs control the somatic excitability and initiation of APs (Miles et al, 1996). For example, an *in vivo* study (Royer et al., 2012) reveals that dendrite-targeting SST^+ INs regulate the firing rate of CA1 pyramidal cells while soma-targeting PV^+ INs control the timing of pyramidal cells spikes. In the DG, soma-targeting FS INs provide reliable and strong inhibition onto GCs in response to cortical inputs (Liu et al., 2014). Dendrite-targeting non-FS INs exert weak inhibition onto GCs during low activity but display powerful and sustained inhibition in

response to a series of intense cortical inputs (Liu et al., 2014). According to our recent work, the PV^+ INs controlled the onset of AP trains in GCs while SST^+ INs regulated the latter phase in response to series of PP stimulation.

In addition to PV^+ INs and SST^+ INs, there are at least three types of INs in the DG, including HICAP, TML and ML cells (Hosp et al., 2014; Hsu et al., 2015). Among them, HICAP and TML cells are known to express CB_1Rs (Halasy and Somogyi, 1993; Tsou et al., 1999; Yu et al., 2015). Therefore, we investigated the role of CB_1R-expressing INs using pharmacological approaches. Pharmacological activation of CB_1Rs with the agonist WIN 55,212-2 decreases the neurotransmission release from CB_1R-expressing terminals (Katona et al., 1999; Katona et al., 2001; Hájos et al., 2002; Takahashi and Castillo, 2006; Chiu and Castillo, 2008). We thus hypothesized suppression of CB_1R^+ IN-mediated neurotransmission could enhance GC activity. To this end, we recorded the GC pSpikes in response to a single stimulation of the PP. In contrast to our hypothesis, the magnitude of pSpike (quantified by the area; see Materials and Methods) decreased after bath application of WIN 55,212-2 (5 μM). Notably, the pSpike areas were greatly reduced (41.1 ± 1.8% of baseline, n = 7; Fig. 4). To exclude the off-target effects of WIN 55,212-2, we also simultaneously monitored the fEPSPs during bath application of WIN 55,212-2. The fEPSPs were unchanged (98.4 ± 0.5% of baseline, n = 7; Fig. 4). To corroborate

the effect of WIN 55,212-2 on CB_1Rs, we performed the same experiments in CB_1R-KO mice and found no obvious change of the pSpike magnitude after WIN 55,212-2 application (86.1 ± 1.7% of baseline, n = 7; Fig. 4). The WIN 55,212-2-induced suppression was indeed mediated by CB_1Rs.

Why does decreasing GABA release from CB_1R^+ INs caused a reduction of GC pSpikes? One possibility is that INs instead of GCs are the major target of CB_1R^+ INs. Thus, the inhibition between CB_1R^+ INs and INs was likely reduced after bath application of WIN 55,212-2. WIN 55,212-2-induced disinhibition of INs, which are targeted by CB_1R^+ INs, may account for the observed suppression of GC activity. To test whether INs are involved in this process, we blocked the GABAergic transmission with the $GABA_A$ receptor antagonist gabazine and reexamined the WIN 55,212-2 effect on GC pSpikes. Indeed, the WIN 55,212-2 effect on GC pSpikes in the presence of 1 μM gabazine was not significantly different from those in CB_1R-KO mice (83.6 ± 0.8% of baseline, n = 7; p = 0.79, one-way repeated-measures ANOVA with *post hoc* Bonferroni's test; Fig. 4). The result indicated that WIN 55,212-2 suppressed the evoked GC pSpikes via GABAergic transmission.

Moreover, we tested the WIN 55,212-2 effect on GC pSpikes in response to trains of stimulation at 10 and 30 Hz. We found that the pSpike responses decreased during 10- and 30-Hz trains (10Hz: n = 11, 30Hz: n = 10; Fig. 5A). Notably, the WIN

55,212-2 yielded the greatest effect on the first pSpikes (Fig. 5A). It is worth noting that there were little pSpikes in response to the fourth and fifth stimuli during 30Hz-trains because of marked synaptic depression of this input (Fig 5A). In striking contrast, WIN 55,212-2 had no effect on all pSpikes in CB_1R-KO mice (n = 6; Fig. 5B) and in WT mice with the presence of gabazine (10 Hz: n = 8, 30Hz: n = 10; Fig. 5C). Finally, we tested the possibility that CB_1R is activated by endogenous endocannabinoids during cortical stimulation. To test this notion, we examined the effect of the CB_1R antagonist AM251 (5 μM) on GC pSpikes and found that the pSpike magnitude was not significantly different after AM251 (10Hz: n = 7, 30Hz: n = 6; p = 0.77, two-way repeated-measures ANOVA; Fig. 5D). It suggests that there were not tonic endocannabinoid signaling in our system. Together, these results show that activation of CB_1Rs by WIN 55,212-2 led to decrease GC pSpikes and it required GABAergic transmission.

The CB_1R agonist WIN 55,212-2 has no effect on PP transmission and GC excitability

Both excitatory and inhibitory synapses can be modulated by endocannabinoid signaling (Katona et al., 1999; Katona et al., 2001; Hájos et al., 2002; Takahashi and Castillo, 2006; Chiu and Castillo, 2008). Speaking of excitatory synapses in the DG, endocannabinoids suppress glutamatergic inputs from hilar mossy cells but not those

from layer II entorhinal cortex neurons (Monory et al., 2006, Chiu and Castillo, 2008). Unlike the DG, endocannabinoids modulate the glutamatergic PP inputs from cortical layer III to the CA1 region (Xu et al., 2010). To exclude the direct effect of WIN 55,212-2 on excitatory transmission at the PP-GC synapses, we recorded either EPSCs or fEPSPs in the presence of gabazine. Because mature GCs mainly contribute to GC pSpikes, we recorded evoked EPSCs from GCs with input resistances less than 500 MΩ, a striking feature of mature GCs (Dieni et al., 2013). Consistent with previous studies, the EPSCs evoked by the PPs were unaltered after WIN 55,212-2 application (96.9 ± 1.2% of baseline, n = 8; p = 0.74, Wilcoxon signed rank test; Fig. 6A, B). The paired-pulse ratio (PPR) was not changed after WIN 55,212-2 application (n = 8, p = 0.68, Wilcoxon signed rank test; Fig. 6C). Aside from the responses in single GCs, WIN 55,212-2 did not reduce the amplitude (97.5 ± 0.4% of baseline, n = 6; p = 1.00, Wilcoxon signed rank test; Fig. 6E, F) and slopes of fEPSPs (20-50% slope, 93.8 ± 1.8% of baseline, n = 6; p = 0.31, Wilcoxon signed rank test; Fig. 6G).

Recently, some studies report that endocannabinoids can modulate the intrinsic excitability. In the neocortex, low-threshold spiking inhibitory INs generate a long-lasting self-induced hyperpolarization (Bacci et al., 2004; Marinelli et al., 2008). This self-induced inhibition is mediated by the release of endogenous cannabinoids, which increase K^+ conductance (Bacci et al., 2004; Marinelli et al., 2008). In addition

to inhibitory INs, excitatory pyramidal neurons can synthesize endocannabinoids and express CB_1Rs (Kano et al., 2009; Hill et al., 2007; Fortin and Levine, 2007). Pyramidal neurons also produce endocannabinoid-mediated self-inhibition (Marinelli et al., 2009). Aside from pyramidal neurons in the neocortex, the excitatory GCs can synthesize endocannabinoids but not express CB_1Rs in the DG (Tsou et al., 1998; Egertová and Elphick, 2000; Wager-Miller et al., 2002; Monory et al., 2006). To exclude the WIN 55,212-2 effect on the GC excitability, we analyzed the intrinsic properties of GCs before and after WIN 55,212-2 application. Many representative intrinsic electrical properties, including input resistance (R_{in}), action potential (AP) threshold, AP height, AP half-duration and firing frequency, were not significantly changed by WIN 55,212-2 ($n = 8$; $p = 0.46$ in R_{in} and threshold, $p = 0.64$ in AP height, $p = 0.55$ in AP half-duration, $p = 0.06$ in max. discharge frequency, Wilcoxon signed rank test; Fig. 7). Taken together, our results suggest that WIN 55,212-2 suppresses GC pSpikes through GABAergic transmission.

The CB_1R agonist WIN 55,212-2 increases GABAergic transmission onto GCs

One possible mechanism is that WIN 55,212-2 enhances GABA-mediated inhibitory conductance in GCs. To test this hypothesis, we measured the ratio of inhibitory-excitatory conductance (I/E ratio) in single GCs. With the Cs-based internal

solution, we recorded the IPSCs and EPSCs at 0 mV (close to the EPSC reversal potential) and -50 mV (close to the IPSC reversal potential), respectively. Cs is a non-specific potassium channel blocker, which blocks various K^+ conductances and improves voltage-clamp recording at 0 mV. We found that the I/E ratio increased after WIN 55,212-2 application ($n = 10$; $p < 0.05$, two-way repeated-measures ANOVA with *post hoc* Bonferroni's test; Fig. 8A, B), whereas WIN 55,212-2 had no effect on the I/E ratio in CB_1R-KO mice ($n = 7$; $p = 0.1$, two-way repeated-measures ANOVA; Fig. 8A, B). Notably, the WIN 55,212-2 effect was significantly different at the first stimulation ($p < 0.05$, *post hoc* Bonferroni's test; Fig. 8B). We further analyzed the first responses and plotted the normalized IPSCs ($IPSC_{WIN\ 55,212\text{-}2}/IPSC_{control}$) against the normalized EPSCs ($EPSC_{WIN\ 55,212\text{-}2}/EPSC_{control}$). The majority of the data points in WT mice were scattered upper the dashed line ($IPSC_{WIN\ 55,212\text{-}2}/IPSC_{control} = 1$) compared with those in the CB_1R-KO mice (Fig. 8C). These results suggest that inhibition onto GCs increased relative to excitation after WIN 55,212-2 application, consistent with the WIN 55,212-2-induced reduction in GC pSpikes.

The CB_1R agonist WIN 55,212-2 increases the excitability of basket cells

We next investigated the identities of INs that contributed to the increased inhibition onto GCs after WIN 55,212-2 application. Because WIN 55,212-2 is known to reduce

the neurotransmitter release from CB_1R-expressing terminals (Katona et al., 1999; Katona et al., 2001; Hájos et al., 2002; Takahashi and Castillo, 2006; Hill et al., 2007; Chiu and Castillo, 2008), we proposed that CB_1R^+ INs preferentially target certain types of INs, which provide strong inhibition onto GCs during cortical stimulation. Thus, disinhibition of those INs by WIN 55,212-2 results in the reduction of pSpikes. Among different types of INs in the DG, the BCs present a higher probability coupled by the other INs (Savanthrapadian et al., 2014). The connectivity between the HICAP-BCs is higher than the HIPP-BCs (Savanthrapadian et al., 2014). Besides, BCs are soma-targeting INs, directly regulate AP generation in GCs (Miles et al., 1996). BCs provide the fastest and most robust inhibition onto GCs. The connectivity between BCs to GCs is high and these synapses display strongly short-term depression (Buhl et al., 1995; Bartos and Elgueta, 2012; Savanthrapadian et al., 2014; Liu et al., 2014; Hsu et al., 2015). As shown in previous results (Fig. 5A), the WIN 55,212-2 effect was strongest at the first stimulation during 10-Hz and 30-Hz trains. Thus, we hypothesized that increased activity of BCs accounts for the enhanced inhibition onto GCs.

To test this idea, we examined whether WIN 55,212-2 could enhance the spiking probabilities of BCs in response to cortical stimulation in both WT and CB_1R-KO mice. The BCs in the DG of acute brain slices were identified based on the location of

their cell bodies near the border of the GCL (Fig. 9A), high-frequency AP phenotypes, relatively low input resistance and the absence of sag response upon hyperpolarizing current pulses (Chiang et al., 2010; Hosp et al., 2014; Fig. 9B). Only neurons that generated ≧70 APs per second and had input resistance ≦150 MΩ were selected for experiments. The average input resistance in WT and CB_1R-KO mice were 81.09 ± 8.9 and 67.5 ± 4.0 MΩ, respectively (n = 7 in the WT group, n = 6 in the CB_1R-KO group; Fig. 9D). The average firing rate with 1 nA current injection were 139.0 ± 9.0 Hz in WT mice and 120.6 ± 16.61 Hz in CB_1R-KO mice (n = 7 in the WT group, n = 6 in the CB_1R-KO group; Fig. 9E). Most importantly, all recorded cells were filled with biocytin for *post hoc* reconstruction (Fig. 10). With the GCL as a reference, BCs had the highest axonal density distribution within the GCL (n = 7 in the WT group, n = 6 in the CB_1R-KO group; Fig. 9F, G). Notably, the electrical and morphological properties of BCs were not different in WT and CB_1R-KO mice (p = 0.34 in RMP, p = 0.20 in R_{in}, p = 0.09 in firing frequency, Wilcoxon signed rank test; Fig. 9C-E). An exemplar morphologically confirmed BCs did not generate spikes in response to the 0.03-mA PP stimulation under control conditions, whereas displayed spikes after WIN 55,212-2 application (Fig. 9H). We also obtained the activation curve in response to a range of stimulus intensities. The threshold intensity, which corresponds to the stimulus intensity that elicit 50% spiking probability, was decreased (0.04 mA in the

control group, 0.03 mA in the WIN 55,212-2 group; Fig. 9I). During bath application of WIN 55,212-2, the spiking probabilities of BCs gradually increased and the time course of WIN 55,212-2 effect was similar with Fig. 4B (n = 5; Fig. 9J). To illustrate the changes of individual BCs, we normalized the stimulus intensity to the threshold intensity before WIN 55,212-2 application. We observed that most (6 out of 7) normalized activation curves were shifted toward left, indicating that the threshold decreased after WIN 55,212-2 (n = 7; Fig. 9K). In great contrast, normalized activation curves before and after WIN 55,212-2 application were overlapping in CB_1R-KO mice (n = 6; Fig. 9L). The normalized threshold intensity was obtained from the mid-point of normalized activation curves. WIN 55,212-2 significantly decreased the normalized threshold intensity in WT mice but not those in CB_1R-KO mice ($p < 0.05$, two-way repeated-measures ANOVA with *post hoc* Bonferroni's test; Fig. 9M). Taken together, our results suggest that WIN 55,212-2 disinhibits BC activity in response to the cortical stimulation, which would account for the reduction of GC pSpikes.

PV^+ INs did not participate in WIN 55,212-2-mediated suppression of GC pSpikes

We next tested whether WIN 55,212-2-mediated suppression of GC pSpikes acts through the increase of BC activity. To address this, we examined the WIN 55,212-2

effect on GC pSpikes after silencing PV^+ INs, including the BCs and axon-axonic cells, by optogenetics. This approach is based on a Cre-recombinase-dependent AAV expression system carrying a doubled-floxed *eNpHR3.0-eYFP* to selectively express in transgenic mice expressing Cre recombinase under the control of the PV promoter (Sohal et al., 2009). The NpHR is a chloride ion pump activated by about 590 nm amber light. After activation, NpHR pumps chloride ions into the cells and thus hyperpolarizes the neurons that express it. The double-floxed inverted open reading frame (DIO) viral vectors were used for high specificity and expression levels (Sohal et al., 2009; Fig. 11A).

The viral vectors AAV5-EF1α-DIO-eNpHR3.0-eYFP were bilaterally injected into the ventral DG of the *Pvalb-cre* mice (Fig. 11B). Six weeks after virus injection, hippocampal slices were obtained from those mice for electrophysiological recordings. The strong eYFP signals were detected in the GCL (Fig. 11C). Whole-cell recordings from eYFP-expressing neurons showed that delivery of amber light effectively silenced eYFP-expressing neurons (Fig. 11D, E). We recorded GC pSpikes evoked by the PP stimulation while delivering amber light to silence PV^+ INs at 25 ± 2℃. Silencing of PV^+ INs increased about 1.6 fold of GC pSpike areas (pink squares, 161.2 ± 19.9% of control, n = 8; Fig. 12A-C). As previous results, GC pSpike areas were reduced after WIN 55,212-2 application (black circles, 42.9 ± 2.5% of

$baseline_{control}$, n = 8; Fig. 12B). With silencing of PV^+ INs, the GC pSpike areas were also reduced after WIN 55,212-2 application (pink squares, 61.9 ± 3.5% of $baseline_{control}$, n = 8; Fig. 12B). A similar effect of silencing PV^+ INs on GC pSpikes had been observed after WIN 55,212-2 application (183.7 ± 31.6% of the control+WIN 55,212-2 group, n = 8; Fig. 12C). This result indicated that PV^+ INs could be silenced by amber light during entire experiments.

To compare the effect of light stimulation on WIN 55,212-2-mediated suppression of GC pSpikes, we normalized the pSpike areas to the baseline values of each group. The degree of the WIN 55,212-2-mediated reduction of GC pSpikes was similar between two groups (42.9 ± 2.5% of baseline in the control group versus 43.9 ± 2.5% of baseline in the light group, n = 8; p = 0.87, two-way repeated-measures ANOVA; Fig. 12D). These results indicate that the WIN 55,212-2-mediated reduction of GC pSpikes was not through the enhancement of BC activity. The other types of INs but not BCs might be disinhibited from CB_1R^+ INs and provide stronger inhibition onto GCs after WIN 55,212-2. However, the mechanism underlying the WIN 55,212-2-induced enhancement of BC activity still remains unclear in this study.

Discussion

Summary

In this study, we found that GABAergic INs provide extremely strong inhibition onto GCs and tightly control the activity of GCs. The CB_1R agonist WIN 55,212-2 reduces the GC pSpikes in response to PP stimulation through GABAergic transmission. The possible mechanism underlying the WIN 55,212-2-mediated suppression of GC pSpikes is through the CB_1R^+ INs including HICAP and TML cells that preferentially target INs. After WIN 55,212-2 application, less GABA is released from the CB_1R^+ INs to INs. Thus, the IN activity to cortical stimulation is increased. As a result, GCs receive stronger inhibition, leading to the reduction of GC pSpikes. We also found that the BC activity increases after WIN 55,212-2 application. However, the enhancement of BC activity does not account for WIN 55,212-2-mediated suppression of GC pSpikes. The downstream target of CB_1R^+ INs remains unknown. Furthermore, the underlying mechanism for WIN 55,212-2-induced enhancement of BC activity remains unclear.

Disinhibitory microcircuits in the DG

INs differentially target particular parts of principal cells and form different levels of inhibitory control. Furthermore, INs also target other INs not only providing an

additional degree of control but generating more complicated computational mechanism (Salinas and Thier, 2000; Pouille et al., 2009; Lee et al., 2013; Pi et al., 2013). In the neocortex, an unique type of INs, which expresses vasoactive intestinal polypeptide (VIP), mainly targets INs and thereby specializes in the disinhibitory control. The VIP^+ INs are also named as the “INs specific INs" (Pfeffer et al., 2013). The VIP^+ INs are a relatively small population (~15%) of GABAergic INs compared to PV^+ INs (~40%) and SST^+ INs (~30%) (Miyoshi et al., 2010; Rudy et al., 2011). Recent studies found that VIP^+ INs preferentially innervate SST^+ INs forming the disinhibitory microcircuit in the neocortex and CA1 region of hippocampus (Pfeffer et al., 2013; Pi et al., 2013; Tyan et al., 2014). These disinhibitory microcircuits also involve in the associative learning (Letzkus et al., 2011; Pi et al., 2013; Letzkus et al., 2015). In the DG, the connectivity and function of VIP^+ INs remain unclear. Unlike the neocortex, VIP^+ INs in the DG display heterogeneous morphology. It is worthy to mention that some of the VIP^+ INs in the DG innervate the somata and proximal dendrites of GCs and express CCK (Hajos et al., 1996). Besides, almost 70% of cortical VIP^+ INs express CB_1Rs (Hill et al., 2013). Therefore, we speculate that VIP/CCK-coexpressing INs in the DG is the specific type of CB_1R^+ IN targeting INs. According to our previous study, repetitive stimulation of MPP preferentially recruited HICAP (putatively CCK-expressing) neurons during latter phase of spike

trains (Hsu et al., 2015). Contrary to this notion, we found that WIN 55,212-2 has the maximal effect on the first stimulation. Another possible type of CB_1R^+ INs driving disinhibitory circuits is TML cells. The MPP recruits the TML-like cells at the first stimulation (Hsu et al., 2015). However, the synaptic efficacy of MPP-TML synapses is weaker than MPP-BC synapses and the connection between TMLs and other INs remains unknown. It would be interesting to examine the TML-IN connection and the regulation of WIN 55,212-2 on TML-IN and HICAP-IN synapses.

Possible mechanisms for WIN 55,212-2-induced suppression of GC pSpikes

We found that decreasing GABA release from CB_1R^+ INs with WIN 55,212-2 results in a reduction of GC pSpikes. One explanation for our finding is that CB_1R^+ INs preferentially form functional connections with INs. Thus, the INs would be disinhibited from CB_1R^+ INs and then provide enhanced inhibition onto GCs. As a result, GC pSpikes decrease. Another possibility is that the CB_1R^+ IN to IN synapse forms stronger synaptic efficacy than the CB_1R^+ IN to GC synapse. According to our previous study, the non-FS INs (putative HICAP and TML cells) preferentially formed functional connections with GCs but rarely formed connections with INs in the rat DG (Liu et al., 2014). Although our previous finding is contrary to our hypothesis, we still need to test the specific synaptic strength or connectivity of

CB_1R^+ INs onto GCs and INs. Moreover, another possible mechanism is that CB_1R^+ IN to IN synapses contain higher level of CB_1R than CB_1R^+ IN to GC synapses. In the neocortex and hippocampus, CB_1R is differentially expressed among distinct inputs and show differential modulation by endocannabinoid (Marsicano et al., 2003; Monory et al., 2006; Fortin and Levine, 2007). However, several studies report that the relative densities of CB_1R are not fully reliable indicators of their respective strengths in regulating neurotransmitter release by endocannabinoids. For example, the CB_1R- and CCK-expressing INs can be further classified into two distinct subtypes in the CA1 region. The CCK^+ BCs innervate the perisomatic region of pyramidal cells and the CCK^+ Schaffer collateral-associated cells (CCK^+ SCAs) innervate the pyramidal cell dendrites in the radiatum and oriens layers (Vida et al., 1998; Cope et al., 2002; Pawelzik et al., 2002). CCK^+ BCs and CCK^+ SCAs with similar CB_1R expression level display differential sensitivity of WIN 55,212-2 (Nyíri et al., 2005; Lee et al., 2010). It seems that the downstream signaling of CB_1Rs is more crucial for the efficiency of endocannabinoid control such as the coupling between CB_1Rs and G-proteins or Ca^{2+} channels (Castillo et al., 2012). In addition, the degradative enzymes for endocannabinoids also involve in the regulation of endocannabinoid signaling. The monoacylglycerol lipase (MGL), the major degradative enzyme for 2-AG, controls the duration and magnitude of

depolarization-induced suppression of inhibition/excitation (Blankman et al., 2007; Hashimotodani et al., 2007). Therefore, the differential expression of MGL at CB_1R^+ IN to IN or GC synapses is the other possible mechanism for differential WIN 55,212-2 sensitivity.

CB_1R-dependent effects by WIN 55,212-2 application

Several studies have reported the CB_1R-independent effect of the well-known cannabinoid receptor ligand, WIN 55,212-2. First, WIN 55,212-2 increases the frequency of miniature IPSCs (mIPSCs) recorded from hilar mossy cells in the DG (Hofmann et al., 2011). The WIN 55,212-2 effect on mIPSCs is insensitive to the CB_1R antagonist AM251 and preserves in CB_1R-KO mice (Hofmann et al., 2011). Second, WIN 55,212-2 suppresses the tetraethylammonium-sensitive K^+ current component in the retinal ganglion cells through a CB_1R-independent mechanism (Zhang et al., 2013). Finally, WIN 55,212-2 suppresses the delayed rectifier K^+ and TASK-1 currents in a CB_1R/CB_2R-independent manner in smooth muscle cells (Van den Bossche and Vanheel, 2000; Maingret et al., 2001). Suppression of outward K^+ currents might depolarize the membrane potential and increase the input resistance. In our study, the WIN 55,212-2-mediated suppression of GC pSpikes is abolished in CB_1R-KO mice, indicating a CB_1R-dependent effect of WIN 55,212-2. Furthermore, the spiking probabilities of BCs in CB_1R-KO mice do not change after WIN 55,212-2

application. Further investigation into the WIN 55,212-2 effect on the excitability of INs is required.

Endocannabinoid signaling and behavior

An appropriate response for emotion and stress is important for survival. It requires the fine-tuned regulation of different neural circuits in the brain. The endocannabinoid signaling is one of the regulatory mechanisms (Häring et al., 2012). Indeed, CB_1Rs are highly expressed in the brain regions involved in regulation of emotional responses (Marsicano and Lutz, 1999; Mackie, 2005). Several studies have reported that the endocannabinoid signaling regulates emotion, stress, memory and cognitive function (Viveros et al., 2007). Results obtained from the CB_1R-KO mice and by using CB_1R selective antagonists and inhibitors suggest endocannabinoid signaling regulation of stress responses and anxiety (Viveros et al., 2007; Häring et al., 2012). A lack of CB_1R or CB_1R blockade elevates the anxiety and enhanced the social discrimination (Zimmer et al., 1999; Litvin et al., 2013). At the cellular level, the expression of two major endogenous ligands, 2-AG and arachidonic acid anandamide (AEA), is altered in several brain regions after chronic stress (Patel et al., 2005; Bowles et al., 2012). Interestingly, changes in CB_1R expression levels and impairment of CB_1R function in GABAergic synapses are also observed in the hippocampus after exposure to chronic stress (Reich et al., 2009; Hu et al., 2011). It would be valuable to

investigate the function of CB_1R^+ INs, such as CCK^+ INs, on anxiety- and stress-related behaviors.

In addition to emotion and stress, endocannabinoid signaling also involves in the associative fear learning. Animals lacking of CB_1R or given CB_1R blockers display impaired fear extinction (Marsicano et al., 2002). Similarly, the transgenic mice with CB_1R specific deletion in GABAergic INs, show normal acquisition and expression in associative fear learning but fail to learn fear extinction (Brown et al., 2014). Because fear extinction circuits involve the amygdale, prefrontal cortex, hippocampus and other brain regions (Maren et al., 2013; Tovote et al., 2015), it would be interesting to explore the effect of silencing CB_1R^+ INs, including HICAP- and TML-like interneurons, on fear learning and extinction.

Future work

In this study, we propose that CB_1R^+ INs preferentially target the other INs. Thus, WIN 55,212-2 leads to a disinhibition of the target INs which in turn provide increased inhibition onto GCs. As a result, the GC pSpikes decrease. However, there has been no direct evidence that WIN 55,212-2 reduces the evoked IPSCs in the INs. At first, we could test whether INs receive the feedforward inhibition in response to PP stimulation. Next, we further examine whether WIN 55,212-2 would reduce the feedforward inhibition onto those INs. Finally, we could compare the WIN 55,212-2

effect on feedforward inhibition onto the GCs and INs. Furthermore, using paired recording of synaptically connected INs is a more powerful approach to test whether the CB_1R^+ INs preferentially target the other INs. In addition to the evoked IPSCs, another possibility is to test WIN 55,212-2 effect on the spontaneous IPSC in the INs and GCs.

As previously mentioned, some of the CCK^+ INs and VIP^+ INs also express CB_1Rs. We could investigate the influence of CCK^+ INs and VIP^+ INs-mediated inhibition onto GC pSpikes. To address this, we could inject the viral vectors AAV5-EF1α-DIO-eNpHR3.0-eYFP into ventral DG of *CCK-cre* and *VIP-cre* mice. Thus, we could examine the input-output transformation of GCs after silencing those INs.

國立陽明大學 NATIONAL YANG-MING UNIVERSITY

Figures

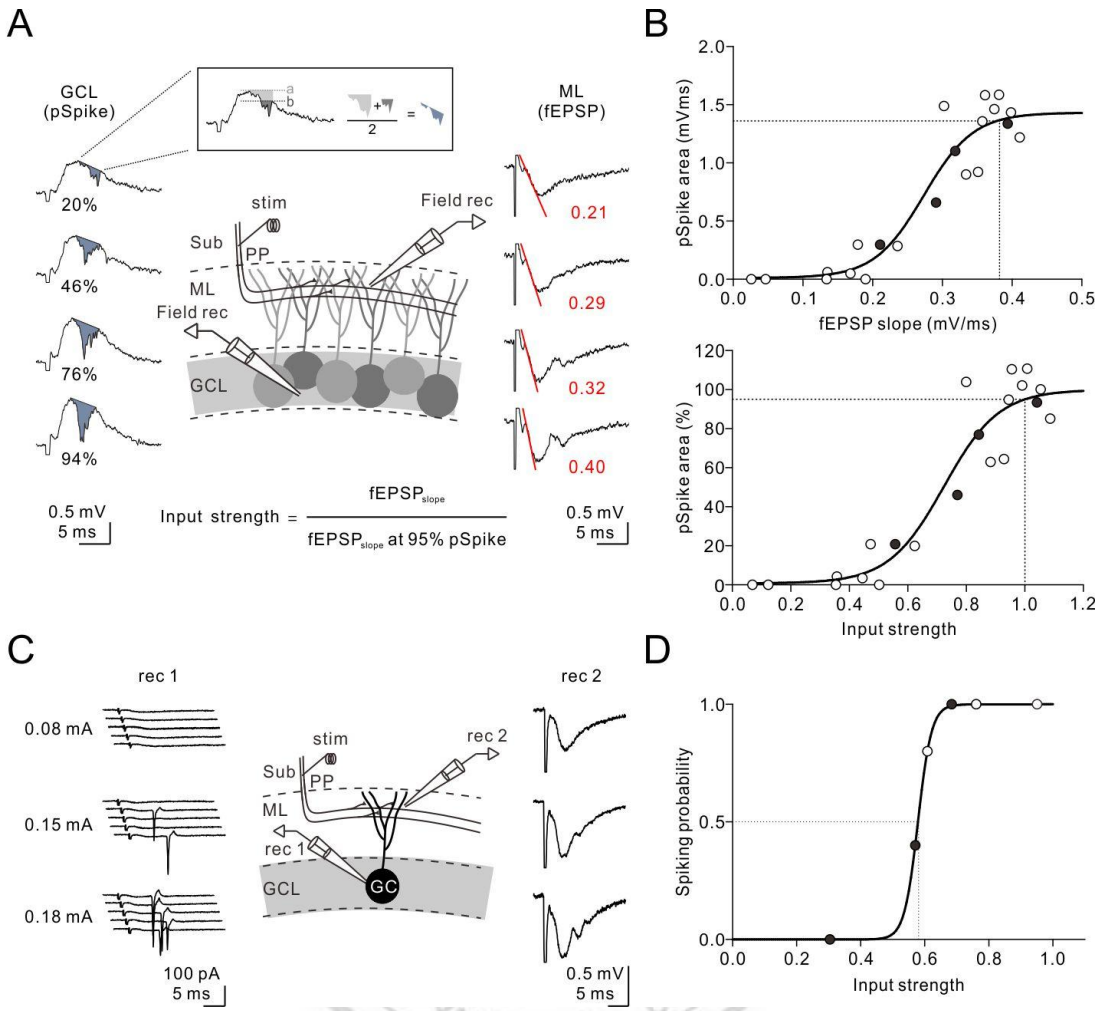

Figure 1. Calibration of input strength for GC activation.

(A) Schematic of recording configuration: a stimulation electrode (stim) was placed in the Sub to activate the PP fibers; two field recording electrodes (glass pipettes filled with ACSF) were placed in the GCL and in the ML to simultaneously detect the pSpike (left) and fEPSP (right), respectively, in response to single pulse delivered to the PP at varying stimulus strengths. The pSpike was calculated by the area (in gray), as measured by the average value of the area below the dashed line a and b (inset).

The input strength is the slope of the fEPSP ($fEPSP_{slope}$; red lines) elicited at any given stimulus intensity normalized to the $fEPSP_{slope}$ evoked at a stimulus intensity, which results in a pSpike of 95% of its maximal amplitude.

(B) Top, the pSpike area is plotted against fEPSP slope for the experiment illustrated in (A). Bottom, the normalized pSpike area is plotted against input strength for the same experiment. Data are fit with a sigmoid function. Filled symbols correspond to the example traces in (A).

(C) Schematic of recording configuration: a stimulation electrode (stim) was placed in the Sub to activate the PP; rec 1 represents the cell-attached recording from a single GC; rec 2 represents field excitatory postsynaptic potential (fEPSP) recording placed in the molecular layer (ML). Example traces of action currents (left) recorded from a single GC in the cell-attached configuration and fEPSP recordings (right) in response to PP stimulation with increasing stimulus intensities (from 0.08 to 0.18 mA, 0.1 ms). Stimulus artifacts are truncated for clarity.

(D) Spiking probability is plotted against input strength for a typical example of a GC fit with a sigmoid curve. Dashed lines indicate the threshold input strength yielding 50% spiking probability of the GC. Filled symbols correspond to the example traces.

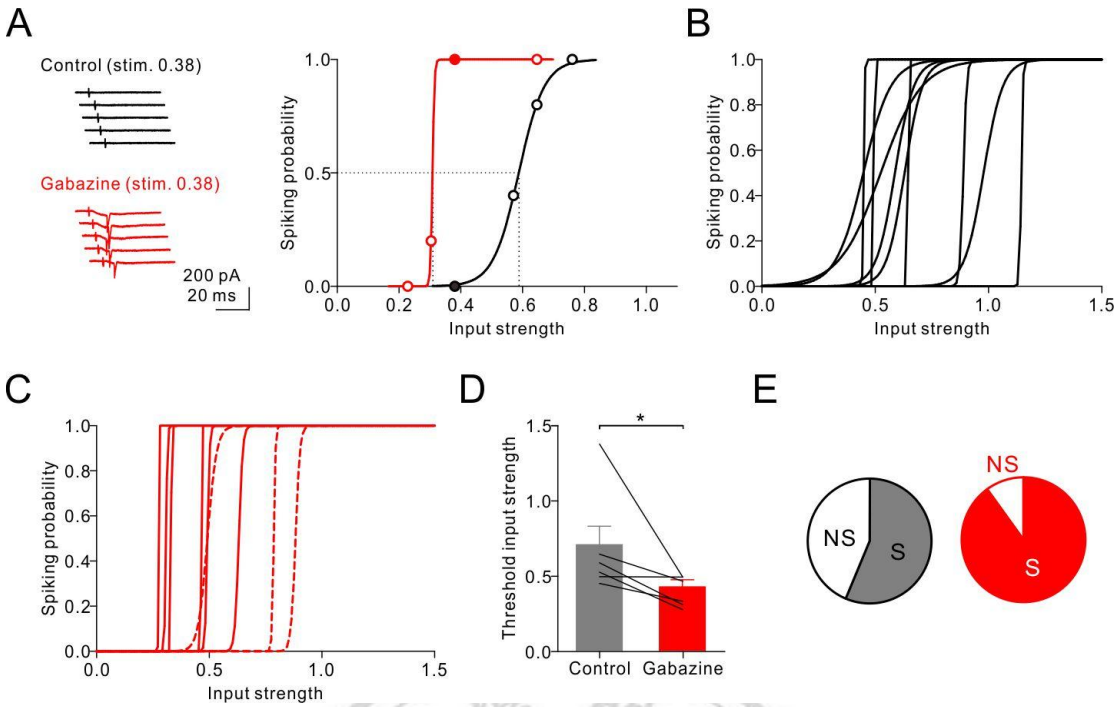

Figure 2. Blockade of $GABA_A$ conductance reduces GC spiking threshold.

(A) Left, cell-attached recording at 0.38 input strength before (black) and after (red) gabazine treatment, 5 consecutive sweeps for each condition. Filled symbols correspond to the example traces. Right, spiking probability for one GC plotted against input strength before (black) and after (red) 1 μM gabazine treatment (sigmoidal fit).

(B) Black sigmoid curves indicate the activation curves of the 10 individual GCs.

(C) Red sigmoids curves indicate the spiking probability of the spiking GCs (n = 6) plotted against input strength after gabazine treatment. Dashed sigmoids indicate the spiking probability of the spiking GCs (n = 3), which were non-spiking GCs before gabazine treatment.

(D) Gray and red bars show the average threshold input strength from GCs before and after gabazine treatment, respectively. *$p < 0.05$

(E) The pie charts show the percentage of spiking (S) and non-spiking (NS) GCs under PP stimulation before (black, NS : S = 7: 9) and after gabazine treatment (red, NS : S = 1: 9), respectively.

國立陽明大學 NATIONAL YANG-MING UNIVERSITY

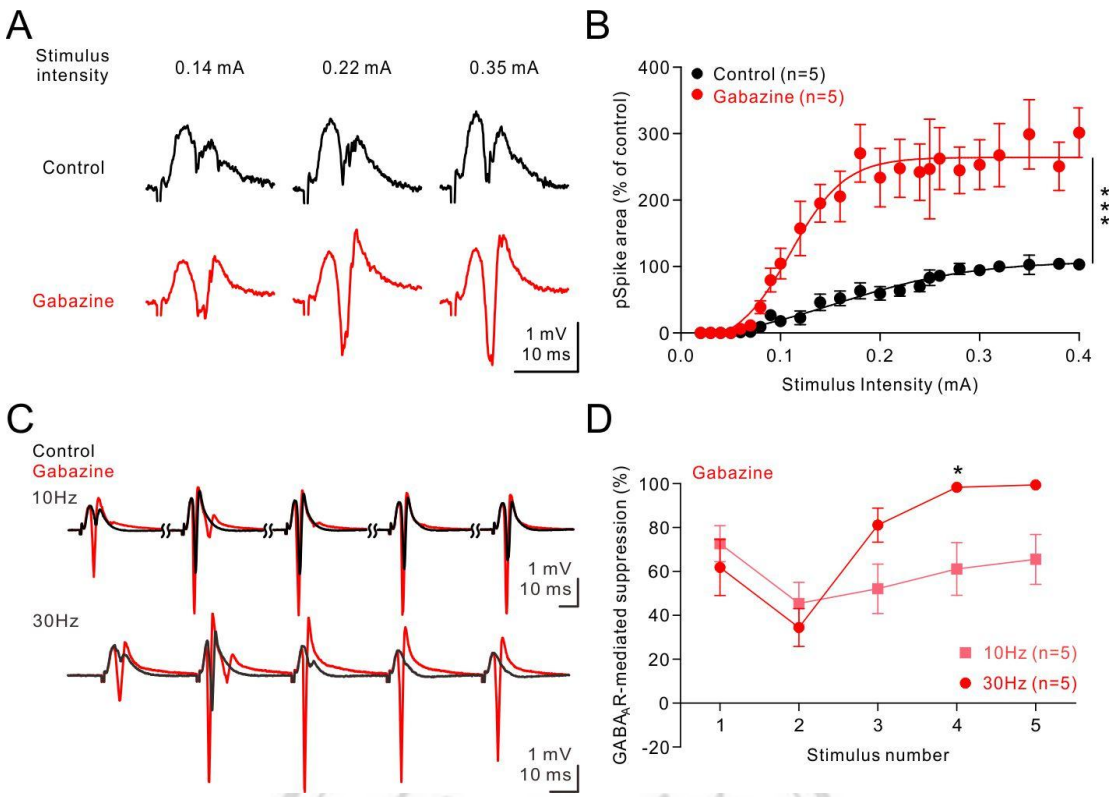

Figure 3. GABA$_A$ conductance regulates the GC input-output transformation.

(A) Field recordings of pSpikes (denoted by the downward deflection) from the GCL in control conditions (black) or after gabazine application (red) at three different stimulus intensities.

(B) The pSpike area is plotted against stimulus intensity under control conditions (black) or after gabazine application (red). Sigmoidal fit to the data-points. ***p < 0.001

(C) pSpikes were evoked by PP stimulation at 10-Hz (top) and 30-Hz (bottom) trains before (black) and after gabazine application (red). Plateau stimulation intensity was used to evoke maximal pSpikes.

(D) Summary plot of $GABA_A$-mediated suppression versus stimulus number. $GABA_AR$-mediated suppression (%) is quantified by 100 × ($pSpike_{gabazine}$ - $pSpike_{control}$)/$pSpike_{gabazine}$. *$p < 0.05$

國立陽明大學 NATIONAL YANG-MING UNIVERSITY

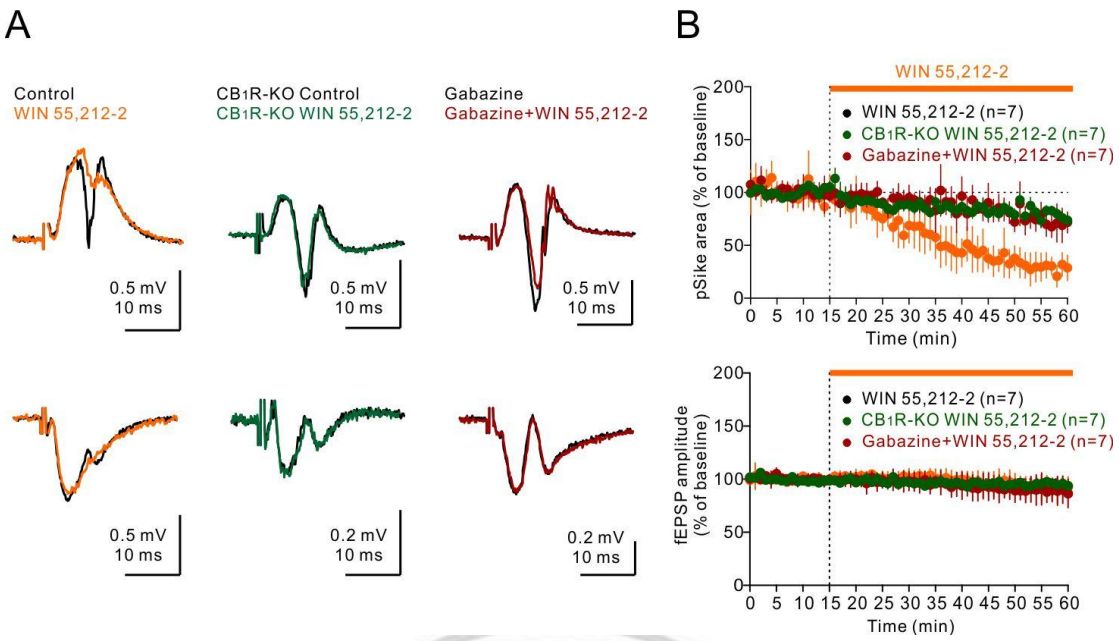

Figure 4. WIN 55,212-2 effect on GC pSpikes.

(A) Top, representative average pSpike traces recorded from the GCL obtained 10 minutes before (black) and 30-40 minutes after 5 μM WIN 55,212-2 application in WT mice (orange), CB_1R-KO mice (green) and in WT mice with the presence of gabazine (brown). Bottom, representative average fEPSP traces simultaneously recorded from the ML.

(B) Summary plots of average pSpike areas (top) and fEPSPs (bottom) against time. Orange bar indicates the application of WIN 55,212-2.

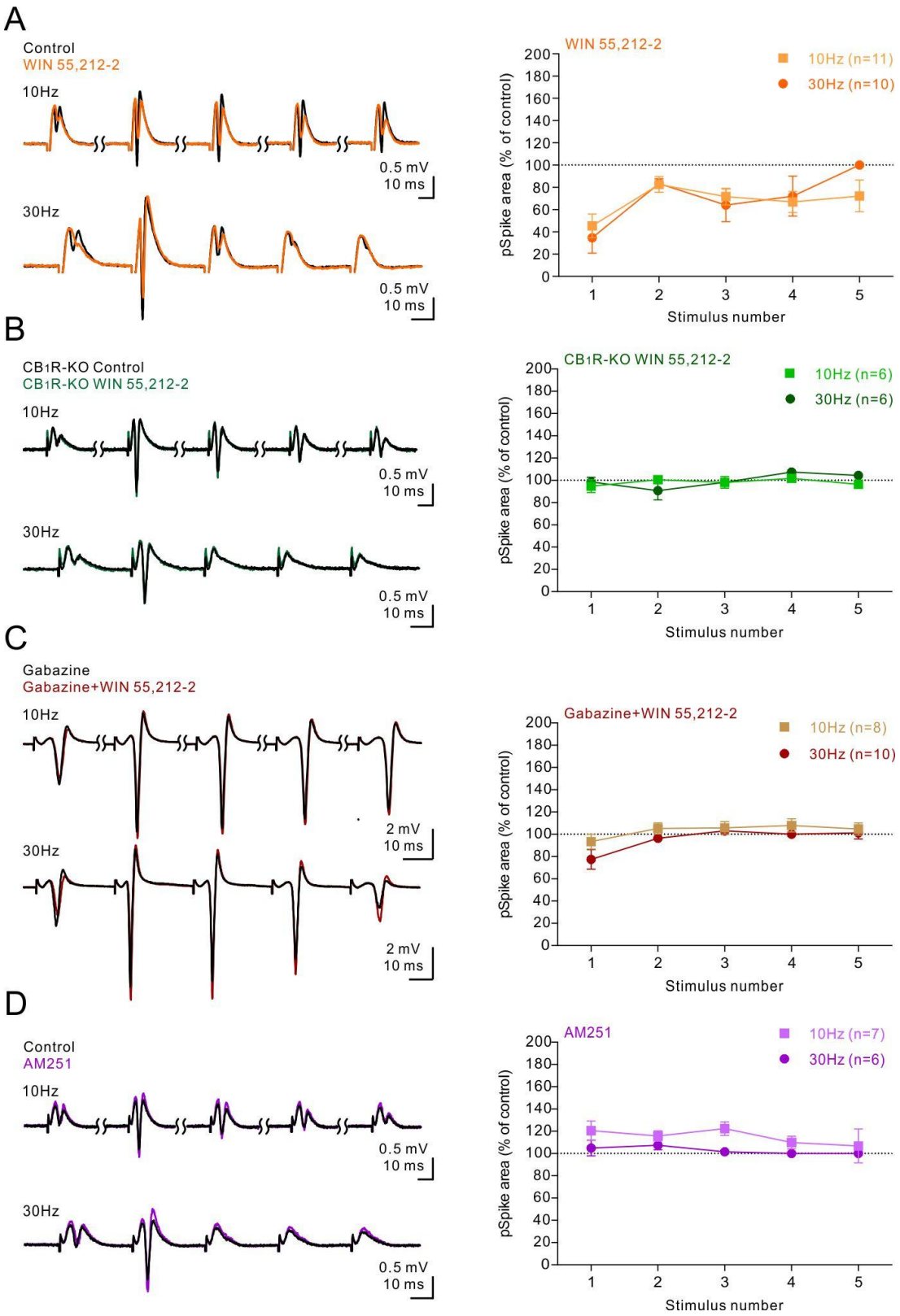

Figure 5. CB_1R-mediated effect on GC pSpike series.

(A) Left, pSpikes evoked by PP stimulation at 10-Hz (top) and 30-Hz (bottom) trains before (black) and after WIN 55,212-2 application (orange). Right, summary plot of normalized pSpike areas versus stimulus number.

(B) Left, pSpikes evoked by PP stimulation at 10-Hz (top) and 30-Hz (bottom) trains before (black) and after WIN 55,212-2 application (green) in the CB_1R-KO mice. Right, summary plot of normalized pSpike areas versus stimulus number.

(C) Left, pSpikes evoked by PP stimulation at 10-Hz (top) and 30-Hz (bottom) trains before (black) and after WIN 55,212-2 application (brown) in WT mice with the presence of gabazine. Right, summary plot of normalized pSpike areas versus stimulus number.

(D) Left, pSpikes evoked by PP stimulation at 10-Hz (top) and 30-Hz (bottom) trains before (black) and after CB_1R antagonist AM251 (5 μM, purple). Right, summary plot of normalized pSpike areas versus stimulus number.

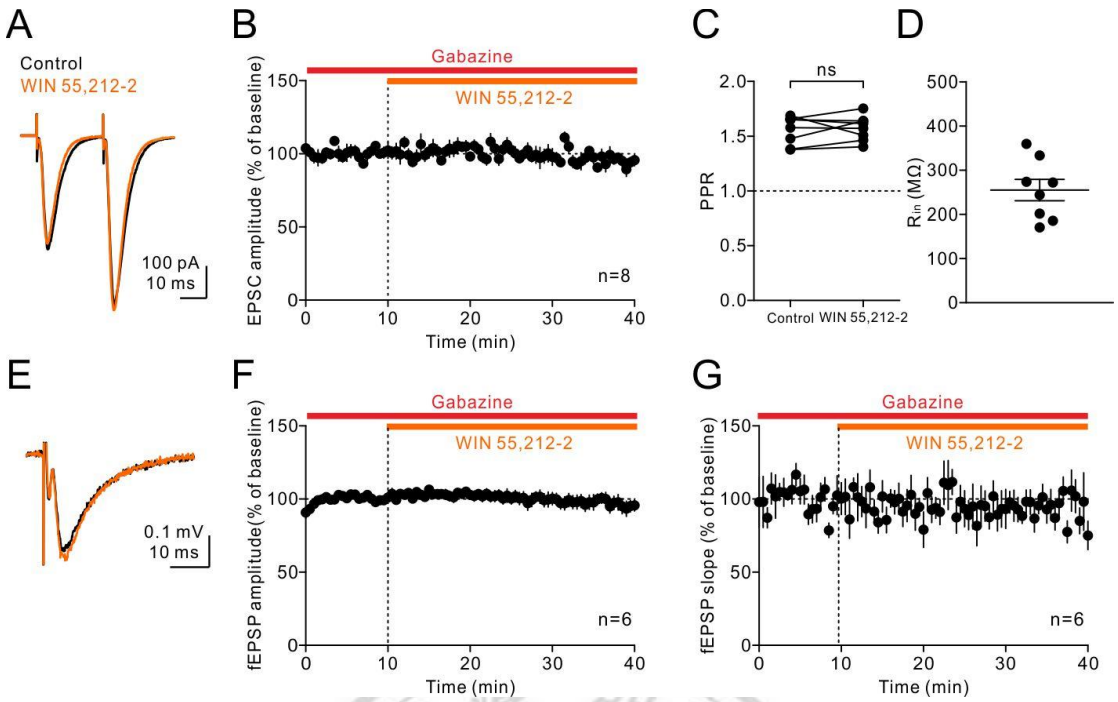

Figure 6. WIN 55,212-2 has no effect on excitatory transmission at PP-GC synapses.

(A) Representative EPSC traces from individual GCs obtained 10 minutes before (black) and 20-30 minutes after WIN 55,212-2 application in the presence of gabazine.

(B) Summary plot of average EPSCs against time. Red and orange bars indicate the application of gabazine and WIN 55,212-2, respectively.

(C) Summary plot of the paired-pulse ratio (PPR) before and after WIN 55,212-2 application. ns indicates no significant difference.

(D) Input resistance (R_{in}) of the recorded GCs.

(E) Representative fEPSP traces obtained 10 minutes before (black) or 20-30 minutes after WIN 55,212-2 application in the presence of gabazine.

(F-G) Summary plot of average fEPSP amplitudes (*F*) and 20-50% slopes (*G*) against time. Red and orange bars indicate the application of gabazine and WIN 55,212-2, respectively.

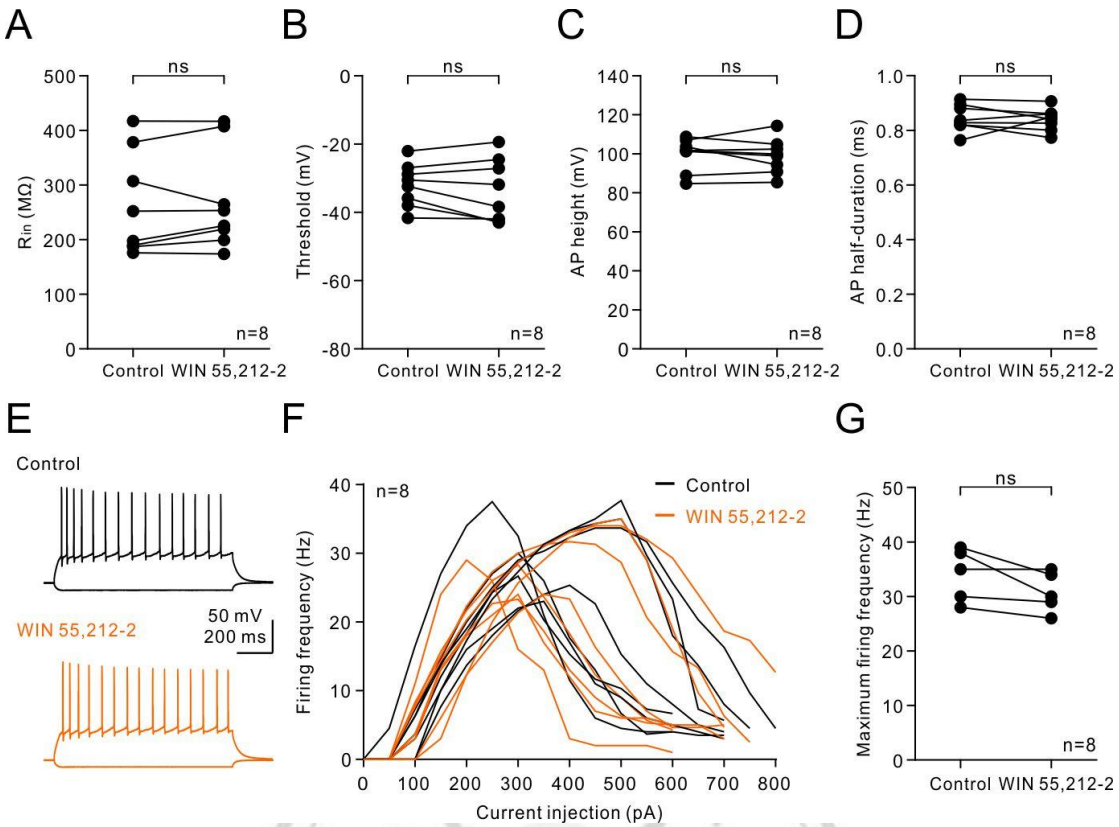

Figure 7. WIN 55,212-2 has no effect on intrinsic properties of GCs.

(A-D) Bar graphs summarize the WIN 55,212-2 effect on four intrinsic properties, including R_{in}, threshold, AP height and AP half-duration, in the presence of synaptic blockers (1 μM gabazine and 2 mM kynurenic acid). ns indicates no significant difference.

(E) Representative voltage responses during 1s long -50 and 150 pA current injections before (black) and after WIN 55,212-2 application (orange)

(F) Frequency-current curves of individual GCs before (black) and after WIN 55,212-2 application (orange).

(G) Maximum firing frequency before and after WIN 55,212-2 application. ns indicates no significant difference.

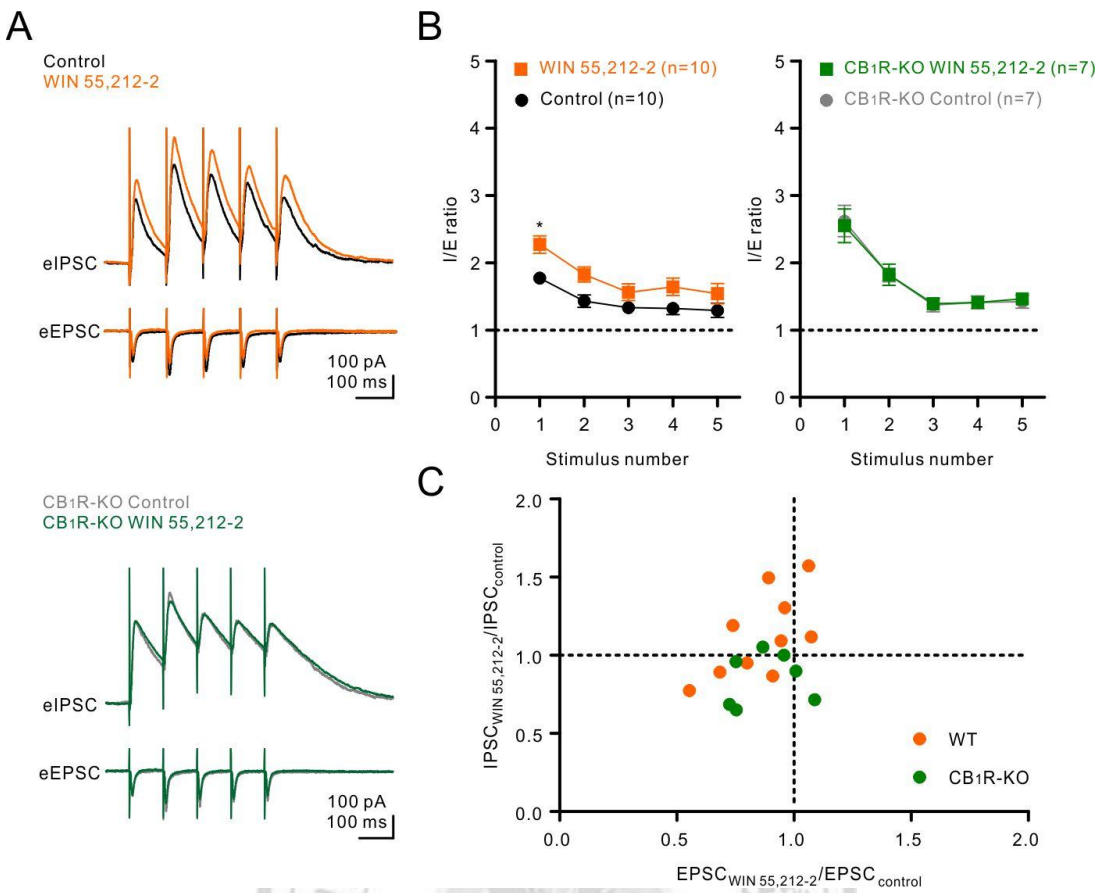

Figure 8. WIN 55,212-2 increases I/E ratio at PP-GC synapses.

(A) Top, representative traces of evoked IPSCs (eIPSC) and EPSCs (eEPSC) recorded in GCs evoked by 10-Hz PP stimulation before (black) and after WIN 55,212-2 application (orange) in WT mice. Bottom, representative traces of evoked IPSCs (eIPSC) and EPSCs (eEPSC) recorded in GCs evoked by 10-Hz PP stimulation before (black) and after WIN 55,212-2 application (green) in CB_1R-KO mice.

(B) Summary plot of the I/E ratio (IPSG/EPSG) versus stimulus number at 10-Hz trains in WT and CB_1R-KO mice. Dashed line indicates the I/E ratio = 1. *$p<0.05$

(C) A scatter plot of normalized EPSCs versus the normalized IPSCs in WT (orange) and CB_1R-KO mice (green), respectively.

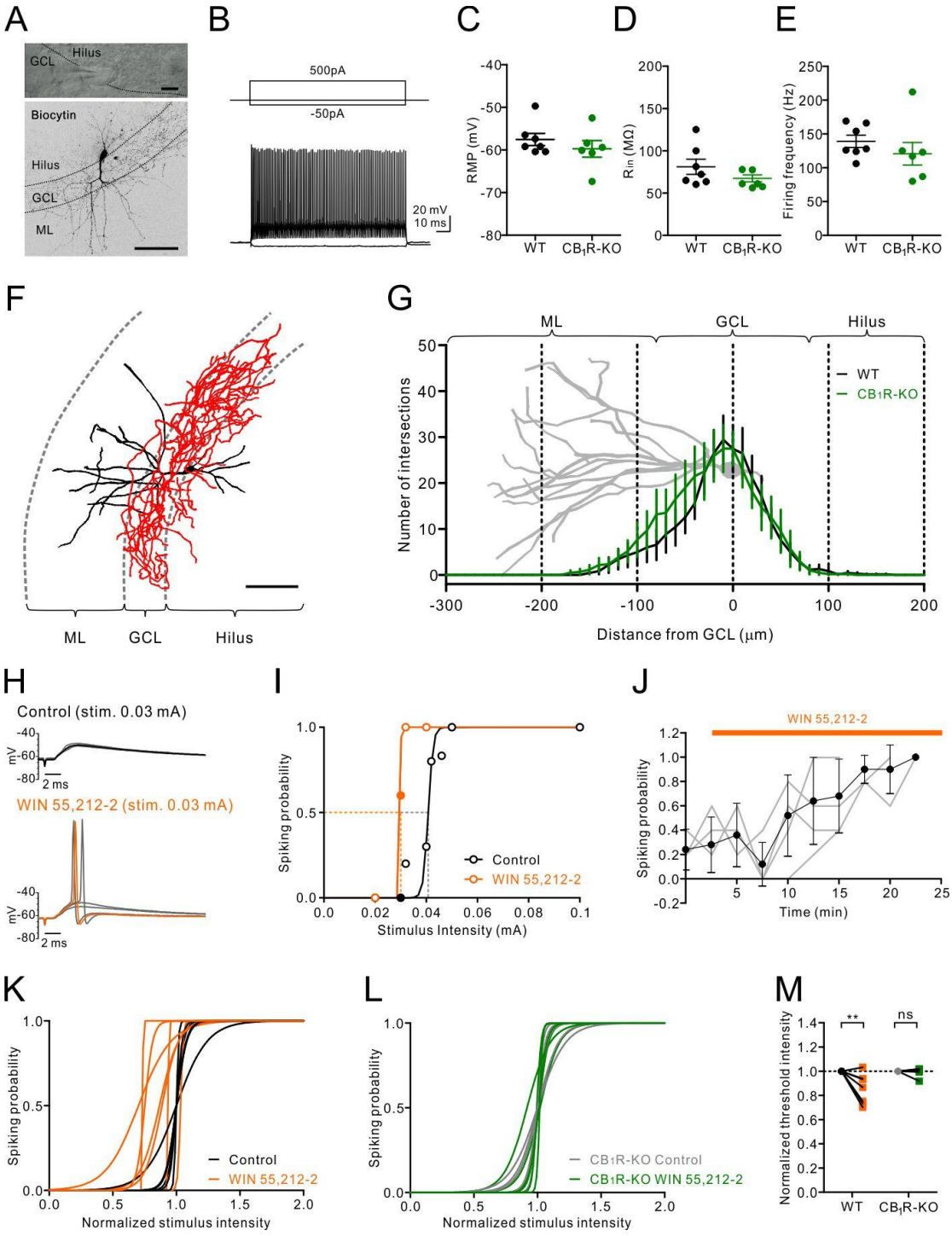

Figure 9. WIN 55,212-2 increases spiking probability of BCs.

(A) Top, IR-DIC image of a BC near the border (dashed line) between the GCL and the hilus in the DG. Scale bar indicates 10 μm. Bottom, two-photon z-stack (maximal intensity) projection of the same BC. Dashed lines demarcate the borders of GCL.

Scale bar indicates 100 µm.

(B) Voltage responses of the same BC shown in (A) to 1 s 500 pA or -50 pA current pulses.

(C-E) The electrophysiological properties of recorded BCs including RMP, R_{in} and firing frequency with 1 nA current injection in WT mice and CB_1R-KO mice, respectively.

(F) Exemplar reconstruction of the BC, which had the major axonal distribution (red) within the GCL. Soma and dendrites are indicated in black. Scale bar indicates 100 µm.

(G) Number of intersections plotted against distance from the GCL. A reconstructed GC (gray) is aligned and scaled to the plot for reference.

(H) Representative traces represent whole-cell recording from a BC in response to PP stimulation at 0.03 mA stimulus intensity before (top, 5 superimposed sweeps) and after WIN 55,212-2 application (bottom). Membrane potential during the recording was held at the resting membrane potential.

(I) Spiking probability of the BC plotted against stimulus intensity before (black) and after (orange) WIN 55,212-2 application (sigmoidal fit). Filled symbols correspond to the representative traces in (H). Dashed lines indicate the threshold stimulus intensity yielding 50% spiking probability.

(J) A plot of spiking probability against time. The black line indicates the mean ± SEM. and the gray lines indicate the individual recordings. Orange bar indicates the application of WIN 55,212-2.

(K) Sigmoids indicate the normalized activation curves before (black) and after (orange) WIN 55,212-2 application in WT mice. The stimulus intensity was normalized to the threshold stimulus intensity before WIN 55,212-2 application.

(L) Sigmoids indicate the normalized activation curves before (black) and after (green) WIN 55,212-2 application in CB_1R-KO mice. The stimulus intensity was normalized to the threshold stimulus intensity before WIN 55,212-2 application.

(M) Summary plot of normalized threshold intensity (normalized to the threshold intensity before WIN 55,212-2 application) before and after WIN 55,212-2 treatment in WT and CB_1R-KO mice, respectively. **$p<0.01$

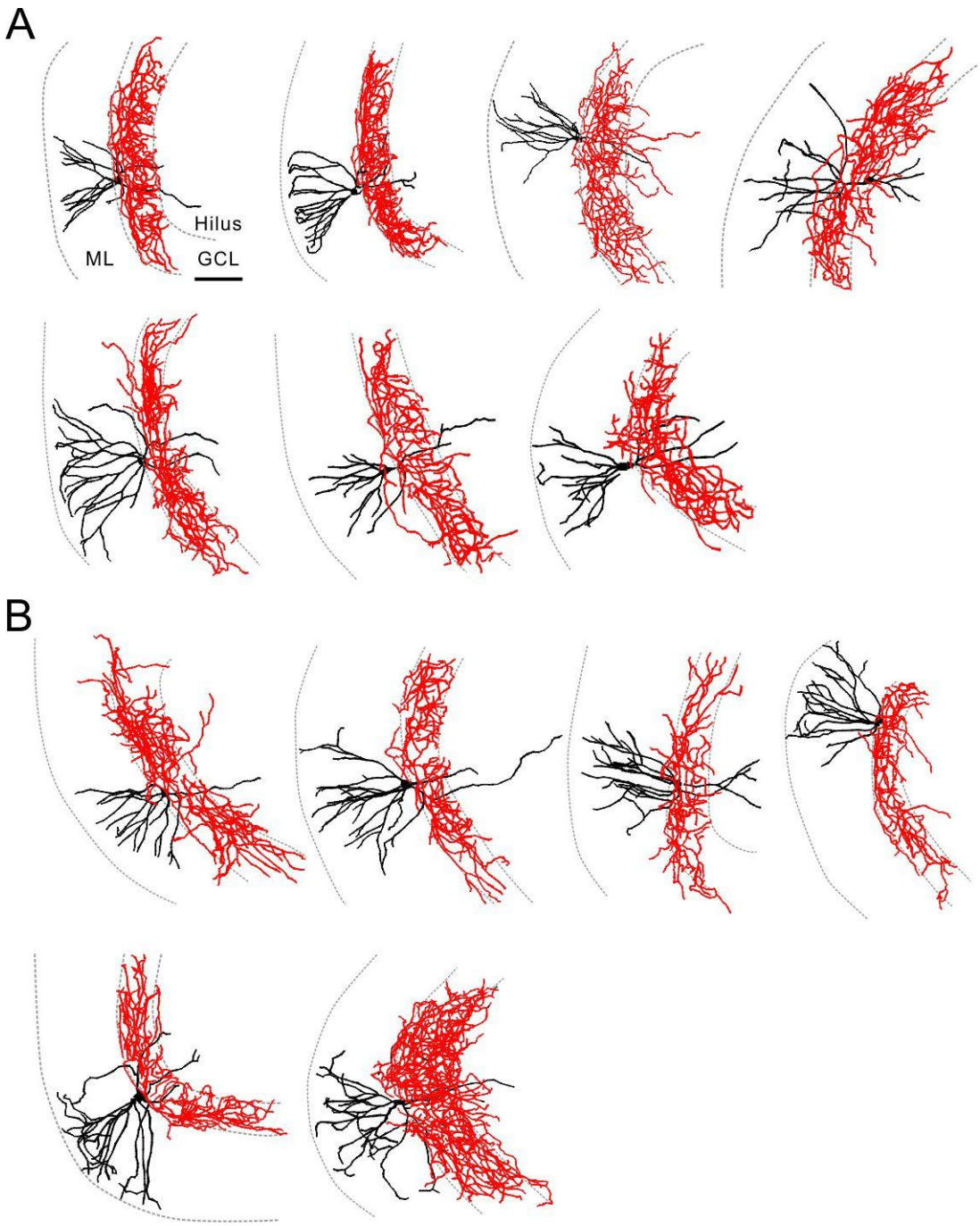

Figure 10. Morphological reconstructions of recorded BCs.

(A-B) Reconstructions of BCs in WT (A) and CB_1R-KO (B) mice. Axons located within the GCL are indicated in red. Soma and dendrites are indicated in black. Scale bar indicates 100 µm.

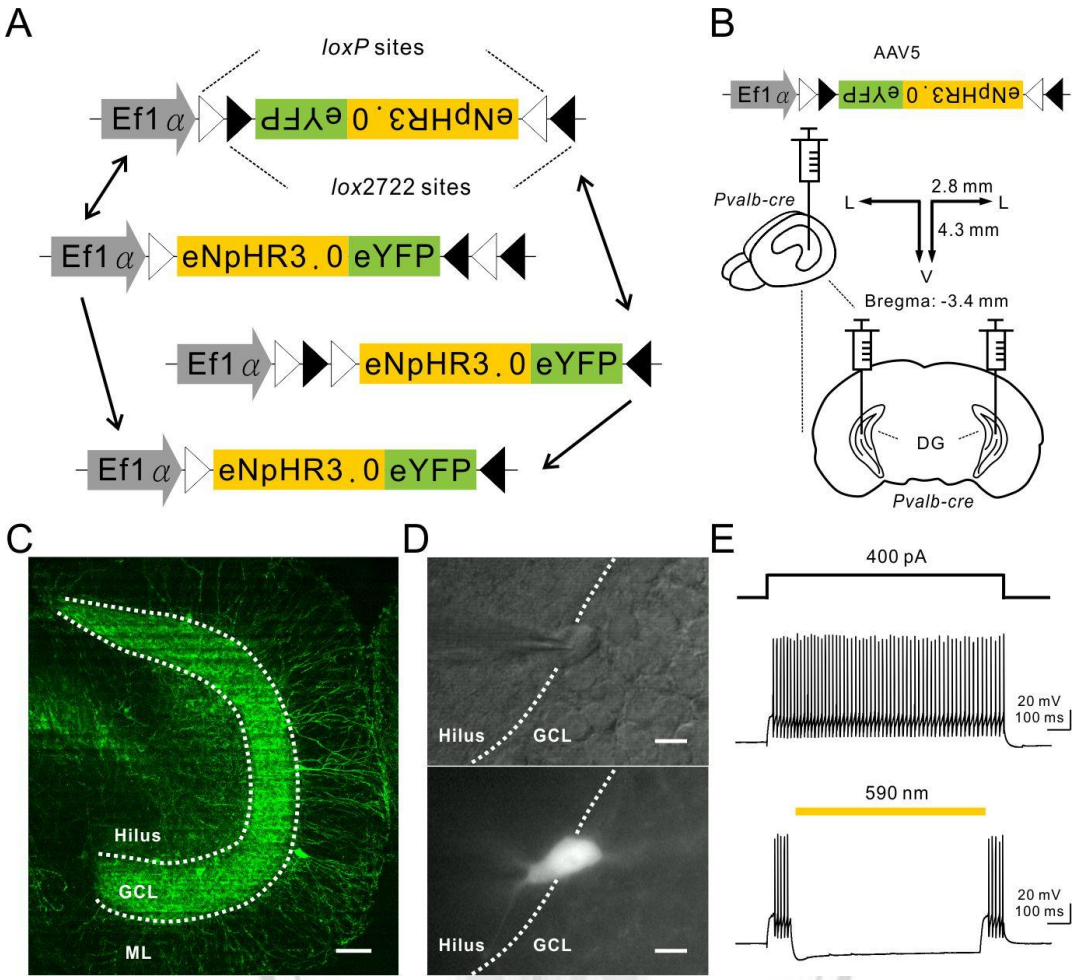

Figure 11. eNpHR-eYFP expression in the PV^{+} cells.

(A) Construction of Cre-dependent AAV5 vectors. Two pairs of incompatible lox sites were used, loxP and lox2722. In the Cre-expressing cells, eNpHR3.0-eYFP was first reversibly flipped into the sense orientation through either pairs of lox sites. After the first step, either pairs of lox sites were in the same direction. Therefore, the sequence between the loxP sites was irreversibly excised.

(B) Schematic diagram illustrates a coronal section from a *Pvalb-cre* mouse injected bilaterally with a viral vector AAV5-EF1α-DIO-eNpHR3.0-eYFP into the DG of the

ventral hippocampus. Axis: L, lateral; V, ventral.

(C) Two-photon image stacks of the ventral DG from *Pvalb-cre* mice 6 weeks after virus injection. Dashed lines demarcate the borders of GCL. Note that the green fluorescent signals were mostly detected in the GCL. Scale bar indicates 100 μm.

(D) IR-DIC image of an eNpHR-eYFP-expressing cell near the border (dashed line) between the GCL and the hilus in the DG. Scale bar indicates 10 μm.

(E) Example spikes evoked by current pulse injection (top) in an eNpHR-eYFP-expressing cell in the absence (middle) and in the presence of optogenetic silencing (bottom).

國立陽明大學 NATIONAL YANG-MING UNIVERSITY

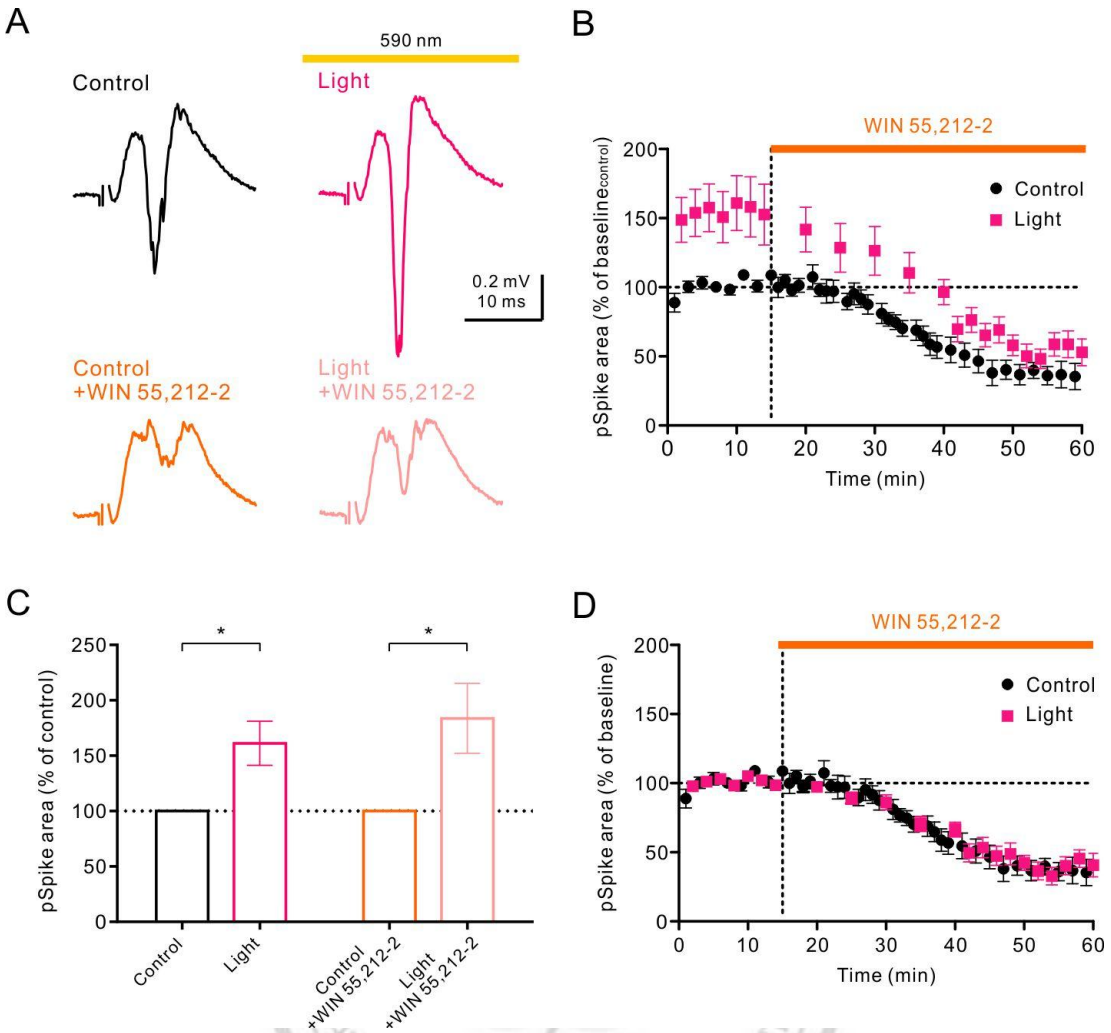

Figure 12. The activity of PV^{+} INs did not contribute to WIN 55,212-2-mediated suppression of GC pSpikes.

(A) Top, field recordings of pSpikes from the GCL in control conditions (black, left) and under light stimulation (pink, right). Bottom, field recordings of pSpikes from the GCL after WIN 55,212-2 application (orange, left) and under light stimulation in the presence of WIN 55,212-2 (light pink, right).

(B) Summary plot of average pSpike areas against time. The black circles and pink squares indicate in the control condition and under light stimulation, respectively.

Orange bar indicates the application of WIN 55,212-2. The pSpike areas were normalized to the baseline in control conditions.

(C) Bar graph of normalized pSpike areas (normalized to the pSpike area without light stimulation) before and after WIN 55,212-2 application, respectively. *$p < 0.05$

(D) Summary plot of normalized pSpike areas against time. The black circles represented in control conditions. The black circles and pink squares indicate in the control condition and under light stimulation, respectively. Orange bar indicates the application of WIN 55,212-2. The pSpike areas were normalized to the baseline value for each group.

國立陽明大學 NATIONAL YANG-MING UNIVERSITY

References

Acsády L, Káli S (2007) Models, structure, function: the transformation of cortical signals in the dentate gyrus. Prog Brain Res 163:577–99.

Allen K, Monyer H (2015) Interneuron control of hippocampal oscillations. Curr Opin Neurobiol 31:81–7.

Amaral DG, Scharfman HE, Lavenex P (2007) The dentate gyrus: fundamental neuroanatomical organization (dentate gyrus for dummies). Prog Brain Res 163:3–22.

Andersen P, Morris R, Amaral D, Bliss T, and O'Keefe J (2007) The Hippocampus Book. Oxford University Press.

Aimone JB, Deng W, Gage FH (2011) Resolving new memories: a critical look at the dentate gyrus, adult neurogenesis, and pattern separation. Neuron 70(4):589–96.

Bartos M, Elgueta C (2012) Functional characteristics of parvalbumin- and cholecystokinin-expressing basket cells. J Physiol 590:669–81.

Bacci A, Huguenard JR, Prince DA (2004) Long-lasting self-inhibition of neocortical interneurons mediated by endocannabinoids. Nature 431(7006):312–6.

Behr J, Lyson KJ, Mody I (1998) Enhanced propagation of epileptiform activity through the kindled dentate gyrus. J Neurophysiol 79:1726–1732.

Blankman JL, Simon GM, Cravatt BF (2007) A comprehensive profile of brain enzymes that hydrolyze the endocannabinoid 2-arachidonoylglycerol. Chem Biol 14(12):1347–56.

Bowles NP, Hill MN, Bhagat SM, Karatsoreos IN, Hillard CJ, McEwen BS (2012) Chronic, noninvasive glucocorticoid administration suppresses limbic endocannabinoid signaling in mice. Neuroscience 204:83–9.

Brown JA, Horváth S, Garbett KA, Schmidt MJ, Everheart M, Gellért L, Ebert P, Mirnics K (2014) The role of cannabinoid 1 receptor expressing interneurons in behavior. Neurobiol Dis 63:210–21.

Brown SP, Brenowitz SD, Regehr WG (2003) Brief presynaptic bursts evoke synapse-specific retrograde inhibition mediated by endogenous cannabinoids. Nat Neurosci 6:1048–1057.

Buhl EH, Cobb SR, Halasy K, Somogyi P (1995) Properties of unitary IPSPs evoked by anatomically identified basket cells in the rat hippocampus. Eur J Neurosci

7(9):1989–2004.

Buzsáki G, Draguhn A (2004) Neuronal oscillations in cortical networks. Science 304(5679):1926–9.

Cajal SR (1893) Estructura del asta de Ammon. Anal Soc Esp Hist Nat (Madrid) 22:53–114.

Caputi A, Melzer S, Michael M, Monyer H (2013) The long and short of GABAergic neurons. Curr Opin Neurobiol 23(2):179–86.

Castillo PE, Younts TJ, Chávez AE, Hashimotodani Y (2012) Endocannabinoid signaling and synaptic function. Neuron 76(1):70–81.

Chancey JH, Poulsen DJ, Wadiche JI, Overstreet-Wadiche L (2014) Hilar mossy cells provide the first glutamatergic synapses to adult-born dentate granule cells. J Neurosci 34(6):2349–54.

Chawla MK, Guzowski JF, Ramirez-Amaya V, Lipa P, Hoffman KL, Marriott LK, Worley PF, McNaughton BL, Barnes CA (2005) Sparse, environmentally selective expression of Arc RNA in the upper blade of the rodent fascia dentata by brief spatial experience. Hippocampus 15:579–586.

Chersi F, Burgess N (2015) The Cognitive Architecture of Spatial Navigation: Hippocampal and Striatal Contributions. Neuron 88(1):64–77.

Chiu CQ, Castillo PE (2008) Input-specific plasticity at excitatory synapses mediated by endocannabinoids in the dentate gyrus. Neuropharmacology 54(1):68–78.

Colombo M, Broadbent N (2000) Is the avian hippocampus a functional homologue of the mammalian hippocampus? Neurosci Biobehav Rev 24(4):465–484.

Cope DW, Maccaferri G, Márton LF, Roberts JDB, Cobden PM, Somogyi P (2002) Cholecystokinin-immunopositive basket and Schaffer collateral-associated interneurones target different domains of pyramidal cells in the CA1 area of the rat hippocampus. Neuroscience 109: 63–80.

Coulter DA, Carlson GC (2007) Functional regulation of the dentate gyrus by GABA-mediated inhibition. Prog Brain Res 163:235–243.

Dieni CV, Nietz AK, Panichi R, Wadiche JI, Wadiche LO (2013) Distinct determinants of sparse activation during granule cell maturation. J Neurosci 33:19131–19142.

Egertová M, Elphick MR (2000) Localisation of cannabinoid receptors in the rat brain using antibodies to the intracellular C-terminal tail of CB. J Comp Neurol 422(2):159–71.

Ewell LA, Jones MV (2010) Frequency-tuned distribution of inhibition in the dentate gyrus. J Neurosci 30:12597–12607.

Fortin DA, Levine ES (2007) Differential effects of endocannabinoids on glutamatergic and GABAergic inputs to layer 5 pyramidal neurons. Cereb Cortex 17(1):163–74.

Halasy K, Somogyi P (1993) Subdivisions in the multiple GABAergic innervation of granule cells in the dentate gyrus of the rat hippocampus. Eur J Neurosci 5:411–429.

Hájos N, Acsady L, Freund TF (1996) Target selectivity and neurochemical characteristics of VIP-immunoreactive interneurons in the rat dentate gyrus. Eur J Neurosci 8(7):1415–31.

Hájos N, Freund TF (2002) Pharmacological separation of cannabinoid sensitive receptors on hippocampal excitatory and inhibitory fibers. Neuropharmacology 43(4):503–10.

Häring M, Guggenhuber S, Lutz B (2012) Neuronal populations mediating the effects of endocannabinoids on stress and emotionality. Neuroscience 204:145–58.

Hashimotodani Y, Ohno-Shosaku T, Kano M (2007) Presynaptic monoacylglycerol lipase activity determines basal endocannabinoid tone and terminates retrograde endocannabinoid signaling in the hippocampus. J Neurosci 27(5):1211–9.

Heifets BD, Castillo PE (2009) Endocannabinoid signaling and long-term synaptic plasticity. Annu Rev Physiol 71, 283–306.

Hill EL, Gallopin T, Férézou I, Cauli B, Rossier J, Schweitzer P, Lambolez B (2007) Functional CB1 receptors are broadly expressed in neocortical GABAergic and glutamatergic neurons. J Neurophysiol 97(4):2580–9.

Hofmann ME, Bhatia C, Frazier CJ (2011) Cannabinoid receptor agonists potentiate action potential-independent release of GABA in the dentate gyrus through a CB1 receptor-independent mechanism. J Physiol 589(15):3801–21.

Hosp JA, Strüber M, Yanagawa Y, Obata K, Vida I., Jonas P, Bartos M (2014) Morpho-physiological criteria divide dentate gyrus interneurons into classes. Hippocampus 24:189–203.

Hsu TT, Lee CT, Tai MH, Lien CC (2015) Differential recruitment of dentate gyrus interneuron types by commissural versus perforant pathways. Cereb Cortex pii: bhv127.

Hu W, Zhang M, Czéh B, Zhang W, Flügge G (2011) Chronic restraint stress impairs endocannabinoid mediated suppression of GABAergic signaling in the hippocampus of adult male rats. Brain Res Bull 85:374–379.

Jang HJ, Park K, Lee J, Kim H, Han KH, Kwag J (2015) $GABA_A$ receptor-mediated feedforward and feedback inhibition differentially modulate the gain and the neural code transformation in hippocampal CA1 pyramidal cells. Neuropharmacology 99:177–86.

Kano M, Ohno-Shosaku T, Hashimotodani Y, Uchigashima M, Watanabe M (2009) Endocannabinoid-mediated control of synaptic transmission. Physiol Rev 89(1):309–80.

Katona I, Sperlágh B, Sík A, Käfalvi A, Vizi ES, Mackie K, Freund TF (1999) Presynaptically located CB1 cannabinoid receptors regulate GABA release from axon terminals of specific hippocampal interneurons. J Neurosci 19(11):4544–58.

Klausberger T, Somogyi P (2008) Neuronal diversity and temporal dynamics: the unity of hippocampal circuit operations. Science 321(5885):53–7.

Knierim JJ (2015) The hippocampus. Curr Biol 25(23):R1116–21.

Krueppel R, Remy S, Beck H (2011) Dendritic integration in hippocampal dentate granule cells. Neuron 71:512–528.

Lee S, Kruglikov I, Huang ZJ, Fishell G, Rudy B (2013) A disinhibitory circuit mediates motor integration in the somatosensory cortex. Nat Neurosci 16(11):1662–70.

Lee SH, Földy C, Soltesz I (2010) Distinct endocannabinoid control of GABA release at perisomatic and dendritic synapses in the hippocampus. J Neurosci 30(23):7993–8000.

Letzkus JJ, Wolff SB, Meyer EM, Tovote P, Courtin J, Herry C, Lüthi A (2011) A disinhibitory microcircuit for associative fear learning in the auditory cortex. Nature 480(7377):331–5.

Letzkus JJ, Wolff SB, Lüthi A (2015) Disinhibition, a circuit mechanism for associative learning and memory. Neuron 88(2):264–76.

Leutgeb JK, Leutgeb S, Moser MB, Moser EI (2007) Pattern separation in the dentate gyrus and CA3 of the hippocampus. Science 315:961–966.

Liu YC, Cheng JK, Lien CC (2014) Rapid dynamic changes of dendritic inhibition in the dentate gyrus by presynaptic activity patterns. J Neurosci 34(4):1344–57.

Litvin Y, Phan A, Hill MN, Pfaff DW, McEwen BS (2013) CB1 receptor signaling regulates social anxiety and memory. Genes Brain Behav 12(5):479–89.

Malykhin NV, Coupland NJ (2015) Hippocampal neuroplasticity in major depressive disorder. Neuroscience 309:200–13.

Maren S, Phan KL, Liberzon I (2013) The contextual brain: implications for fear conditioning, extinction and psychopathology. Nat Rev Neurosci 14(6):417–28.

Marinelli S, Pacioni S, Bisogno T, Di Marzo V, Prince DA, Huguenard JR, Bacci A (2008) The endocannabinoid 2-arachidonoylglycerol is responsible for the slow self-inhibition in neocortical interneurons. J Neurosci 28(50):13532–41.

Marinelli S, Pacioni S, Cannich A, Marsicano G, Bacci A (2009) Self-modulation of neocortical pyramidal neurons by endocannabinoids. Nat Neurosci 12(12):1488–90.

Marsicano G, Lutz B (1999) Expression of the cannabinoid receptor CB1 in distinct neuronal subpopulations in the adult mouse forebrain. Eur J Neurosci 11:4213–4225.

Marsicano G, Goodenough S, Monory K, Hermann H, Eder M, Cannich A, Azad SC, Cascio MG, Gutiérrez SO, van der Stelt M, López-Rodriguez ML, Casanova E, Schütz G, Zieglgänsberger W, Di Marzo V, Behl C, Lutz B (2003) CB1 cannabinoid receptors and on-demand defense against excitotoxicity. Science 302(5642):84–8.

Marsicano G, Wotjak CT, Azad SC, Bisogno T, Rammes G, Cascio MG, Hermann H, Tang J, Hofmann C, Zieglgänsberger W, Di Marzo V, Lutz B (2002) The endogenous cannabinoid system controls extinction of aversive memories. Nature 418(6897):530–4.

Mackie K (2005) Distribution of cannabinoid receptors in the central and peripheral nervous system. Handb Exp Pharmacol (168):299–325.

McBain CJ, Fisahn A (2001) Interneurons unbound. Nat Rev Neurosci 2(1):11–23.

Miles R, Tóth K, Gulyás AI, Hájos N, Freund TF (1996) Differences between somatic and dendritic inhibition in the hippocampus. Neuron 16(4):815–23.

Miyoshi G1, Hjerling-Leffler J, Karayannis T, Sousa VH, Butt SJ, Battiste J, Johnson JE, Machold RP, Fishell G (2010) Genetic fate mapping reveals that the caudal

ganglionic eminence produces a large and diverse population of superficial cortical interneurons. J Neurosci 30(5):1582–94.

Monory K, Massa F, Egertová M, Eder M, Blaudzun H, Westenbroek R, Kelsch W, Jacob W, Marsch R, Ekker M, Long J, Rubenstein JL, Goebbels S, Nave KA, During M, Klugmann M, Wölfel B, Dodt HU, Zieglgänsberger W, Wotjak CT, Mackie K, Elphick MR, Marsicano G, Lutz B (2006) The endocannabinoid system controls key epileptogenic circuits in the hippocampus. Neuron 51(4):455–66.

Moser EI, Kropff E, Moser MB (2008) Place cells, grid cells, and the brain's spatial representation system. Annu Rev Neurosci 31:69–89.

Nitz D, McNaughton B (2004) Differential modulation of CA1 and dentate gyrus interneurons during exploration of novel environments. J Neurophysiol 91:863–872.

Nunzi MG, Gorio A, Milan F, Freund TF, Somogyi P, Smith AD (1985) Cholecystokinin-immunoreactive cells form symmetrical synaptic contacts with pyramidal and nonpyramidal neurons in the hippocampus. J Comp Neurol 237(4):485–505.

Nusser Z, Mody I (2002) Selective modulation of tonic and phasic inhibitions in dentate gyrus granule cells. J Neurophysiol 87(5):2624–2628.

Pernía-Andrade AJ, Jonas P (2014) Theta-gamma-modulated synaptic currents in hippocampal granule cells in vivo define a mechanism for network oscillations. Neuron 81(1):140–52.

Nyíri G, Cserép C, Szabadits E, Mackie K, Freund TF (2005) CB1 cannabinoid receptors are enriched in the perisynaptic annulus and on preterminal segments of hippocampal GABAergic axons. Neuroscience 136(3):811–22.

O'Keefe J, Nadel L (1978) The Hippocampus as a Cognitive Map. Oxford University Press.

Pawelzik H, Hughes DI, Thomson AM (2002) Physiological and morphological diversity of immunocytochemically defined parvalbumin- and cholecystokinin-positive interneurones in CA1 of the adult rat hippocampus. J Comp Neurol 443:346–367.

Patel S, Kingsley PJ, Mackie K, Marnett LJ, Winder DG (2009) Repeated homotypic stress elevates 2-arachidonoylglycerol levels and enhances short-term endocannabinoid signaling at inhibitory synapses in basolateral amygdala. Neuropsychopharmacology 34:2699–2709.

Pfeffer CK, Xue M, He M, Huang ZJ, Scanziani M (2013) Inhibition of inhibition in visual cortex: the logic of connections between molecularly distinct interneurons. Nat Neurosci 16(8):1068–76.

Pi HJ, Hangya B, Kvitsiani D, Sanders JI, Huang ZJ, Kepecs A (2013) Cortical interneurons that specialize in disinhibitory control. Nature 503(7477):521–4.

Pouille F, Marin-Burgin A, Adesnik H, Atallah BV, Scanziani M (2001) Input normalization by global feedforward inhibition expands cortical dynamic range. Nat Neurosci 12(12):1577–85.

Pouille F, Scanziani M (2001) Enforcement of temporal fidelity in pyramidal cells by somatic feed-forward inhibition. Science 293:1159–1163.

Pouille F, Scanziani M (2004) Routing of spike series by dynamic circuits in the hippocampus. Nature 429:717–723.

Pouille F, Marin-Burgin A, Adesnik H, Atallah BV, Scanziani M (2009) Input normalization by global feedforward inhibition expands cortical dynamic range. Nat Neurosci 12(12):1577–85.

Reich CG, Taylor ME, McCarthy MM (2009) Differential effects of chronic unpredictable stress on hippocampal CB1 receptors in male and female rats. Behav Brain Res 203:264–269.

Royer S, Zemelman BV, Losonczy A, Kim J, Chance F, Magee JC, Buzsáki G (2012) Control of timing, rate and bursts of hippocampal place cells by dendritic and somatic inhibition. Nat Neurosci 15(5):769–75.

Rudy B, Fishell G, Lee S, Hjerling-Leffler J. (2011) Three groups of interneurons account for nearly 100% of neocortical GABAergic neurons. Dev Neurobiol 71(1):45–61.

Savanthrapadian S, Meyer T, Elgueta C, Booker SA, Vida I, Bartos M (2014) Synaptic properties of SOM- and CCK-expressing cells in dentate gyrus interneuron networks. J Neurosci 34(24):8197–209.

Scharfman HE, Myers CE (2012) Hilar mossy cells of the dentate gyrus: a historical perspective. Front Neural Circuits 6:106.

Schmidt-Hieber C, Jonas P, Bischofberger J (2007) Subthreshold dendritic signal processing and coincidence detection in dentate gyrus granule cells. J Neurosci 27:8430–8441.

Scoville WB, Milner B (1957) Loss of recent memory after bilateral hippocampal lesions. J Neurol Neurosurg Psychiatry 20(1):11–21.

Shatz CJ (1990) Impulse activity and the patterning of connections during CNS development. Neuron 5(6):745–56.

Salinas E, Thier P (2000) Gain modulation: a major computational principal of the central nervous system. Neuron 27(1):15–21.

Sohal VS, Zhang F, Yizhar O, Deisseroth K (2009) Parvalbumin neurons and gamma rhythms enhance cortical circuit performance. Nature 459(7247):698–702.

Somogyi P, Hodgson AJ, Smith AD, Nunzi MG, Gorio A, Wu JY (1984) Different populations of GABAergic neurons in the visual cortex and hippocampus of cat contain somatostatin- or cholecystokinin-immunoreactive material. J Neurosci 4(10):2590–603.

Stell BM, Mody I (2002) Receptors with different affinities mediate phasic and tonic GABA(A) conductances in hippocampal neurons. J Neurosci 22(10):RC223.

Strange BA, Witter MP, Lein ES, Moser EI (2014) Functional organization of the hippocampal longitudinal axis. Nat Rev Neurosci 15(10):655–69.

Takahashi KA, Castillo PE (2006) The CB1 cannabinoid receptor mediates glutamatergic synaptic suppression in the hippocampus. Neuroscience 139(3):795–802.

Tovote P, Fadok JP, Lüthi A (2015) Neuronal circuits for fear and anxiety. Nat Rev Neurosci 16(6):317–31.

Treves A, Tashiro A, Witter MP, Moser EI (2008) What is the mammalian dentate gyrus good for? Neuroscience 154:1155–1172.

Tsou K, Brown S, Sañudo-Peña MC, Mackie K, Walker JM (1998) Immunohistochemical distribution of cannabinoid CB1 receptors in the rat central nervous system. Neuroscience 83(2):393–411.

Tsou K, Mackie K, Sañudo-Peña MC, Walker JM (1999) Cannabinoid CB1 receptors are localized primarily on cholecystokinin-containing GABAergic interneurons in the rat hippocampal formation. Neuroscience 93(3):969–75.

Tyan L, Chamberland S, Magnin E, Camiré O, Francavilla R, David LS, Deisseroth K, Topolnik L (2014) Dendritic inhibition provided by interneuron-specific cells controls the firing rate and timing of the hippocampal feedback inhibitory circuitry. J Neurosci

34(13):4534–47.

Vida I, Halasy K, Szinyei C, Somogyi P, Buhl EH (1998) Unitary IPSPs evoked by interneurons at the stratum radiatum-stratum lacunosum-moleculare border in the CA1 area of the rat hippocampus in vitro. J Physiol 506:755–73.

Viveros MP, Marco EM, Llorente R, López-Gallardo M (2007) Endocannabinoid system and synaptic plasticity: implications for emotional responses. Neural Plast 2007:52908.

Wager-Miller J, Westenbroek R, Mackie K (2002) Dimerization of G protein-coupled receptors: CB1 cannabinoid receptors as an example. Chem Phys Lipids 121(1-2):83–9.

Walker GA (2002) Common statistical methods for clinical research with SAS examples, Ed 2. SAS Institute.

Wilson RI, Kunos G, Nicoll RA (2001) Presynaptic specificity of endocannabinoid signaling in the hippocampus. Neuron 31:453–462.

Xu JY, Chen R, Zhang J, Chen C (2010) Endocannabinoids differentially modulate synaptic plasticity in rat hippocampal CA1 pyramidal neurons. PLoS One 5(4):e10306.

Yu EP, Dengler CG, Frausto SF, Putt ME, Yue C, Takano H, Coulter DA (2013) Protracted postnatal development of sparse, specific dentate granule cell activation in the mouse hippocampus. J Neurosci 33(7):2947–60.

Yu J, Swietek B, Proddutur A, Santhakumar V (2015) Dentate total molecular layer interneurons mediate cannabinoid-sensitive inhibition. Hippocampus 25(8):884–9.

Zhang CQ, Wu HJ, Wang SY, Yin S, Lu XJ, Miao Y, Wang XH, Yang XL, Wang Z (2013) Suppression of outward K^+ currents by WIN55212-2 in rat retinal ganglion cells is independent of CB1/CB2 receptors. Neuroscience 253:183–93.

Zimmer A, Zimmer AM, Hohmann AG, Herkenham M, Bonner TI (1999) Increased mortality, hypoactivity, and hypoalgesia in cannabinoid CB1 receptor knockout mice. Proc Natl Acad Sci USA 96(10):5780–5.